Self- and foreign-atom diffusion in semiconductor isotope heterostructures. II. Experimental results for silicon

H. Bracht*
Institut für Materialphysik, University of Münster, D-48149 Münster, Germany

H. H. Silvestri, I. D. Sharp, and E. E. Haller
Lawrence Berkeley National Laboratory and University of California at Berkeley, Berkeley, California 94720, USA
(Received 15 September 2006; published 17 January 2007)

We report the diffusion of boron, arsenic, and phosphorus in silicon isotope multilayer structures at temperatures between 850 °C and 1100 °C. The diffusion of all dopants and self-atoms at a given temperature is modeled with the same setting of all native-point-defect-related parameters. The evaluation of the relative contributions of charged native-point defects to self-diffusion enables us to determine the defect energy levels introduced by the native-point defects in the Si band gap. Making allowance for the fact that the band gap and the energy levels change with temperature, an energy-level diagram of the native-point defects is obtained that shows a reversed level ordering for the donor levels of the self-interstitials. In accord with the general state of knowledge, the diffusion of boron is mainly mediated by self-interstitials whereas the properties of both vacancies and self-interstitials are important to model arsenic and phosphorus diffusion. The simultaneous diffusion of phosphorus and silicon requires the existence of a singly positively charged interstitial phosphorus. It is the diffusion of this defect that strongly affects the shape of the phosphorus diffusion tail and not entirely the supersaturation of self-interstitials argued so far. Taking into account the mechanisms of dopant diffusion and the properties of native-point defects determined from the simultaneous diffusion experiments, let us describe accurately dopant profiles given in the literature. Altogether, this work provides overall consistent data for modeling dopant and self-diffusion in Si for various experimental conditions. A comparison of experimentally and theoretically determined activation enthalpies of self- and dopant diffusion shows excellent agreement for self-interstitial-mediated diffusion but significant differences for vacancy-mediated diffusion in Si. This disagreement either reflects the deficiency of first-principle calculations to accurately predict the energy band gap of Si or points to a still-remaining lack in our understanding of diffusion in Si.

DOI: 10.1103/PhysRevB.75.035211 PACS number(s): 61.72.Ji, 66.30.Dn, 66.30.Hs, 66.30.Jt

I. INTRODUCTION

The progressive miniaturization of Si electronic devices depends strongly on sharply delineated shallow dopant profiles and high doping concentrations. The maximum solubility of common dopants such as boron (B), phosphorus (P), and arsenic (As) in silicon (Si) is close to or higher than 10^{20} cm^{-3} at typical Si processing temperatures between 800 °C and 1200 °C.[1] As a consequence the free-carrier concentration introduced by doping exceeds the intrinsic-carrier concentration. Electronically extrinsic doping conditions affect the formation of charged-point defects and hence the dopant-diffusion process itself, which involves both dopant atoms and native-point defects. Accordingly, detailed information about diffusion mechanisms and point-defect properties under extrinsic doping conditions are required for predictive modeling of dopant diffusion in Si under various experimental conditions.

The mechanisms of self- and dopant diffusion in Si have been investigated extensively over the past decades. Numerous papers on the diffusion of B, As, P, and antimony (Sb) have been published.[2] Modeling of dopant diffusion taking into account appropriate diffusion mechanisms shows that dopant diffusion in Si is fairly well understood.[3,4] However, the charge states of native-point defects involved in the dopant-diffusion processes are still not known in detail as well as the corresponding relative contributions to self-diffusion.

More detailed information about the properties of native-point defects and the mechanisms of dopant diffusion in Si can be obtained from simultaneous dopant and self-diffusion experiments with isotopically controlled Si multilayer structures (see Part I). These studies, which are the subject of the present work, represent a strict consistency check of our present understanding of dopant diffusion in Si. It is demonstrated that several important aspects of dopant diffusion in Si were and are not correctly understood.

Experiments on the simultaneous self- and dopant diffusion are described in Sec. II. Concentration profiles of B, As, and P and the corresponding Si profiles are shown in Sec. III. The diffusion mechanisms and model parameters considered for modeling the experimental profiles are introduced in Sec. IV. The results obtained from the analysis of dopant diffusion in Si isotope multilayer structures and from dopant profiles in natural Si given in the literature are summarized and discussed in Secs V and VI, respectively. Section VII concludes the paper.

II. EXPERIMENTAL

A Si isotope multilayer structure was grown via chemical-vapor deposition at Lawrence Semiconductor Research Laboratory (Tempe, AZ) on a (100)-oriented B-doped Si substrate wafer with a resistivity higher than 10 Ω cm. The structure consists of a 200-nm-thick Si buffer layer grown on

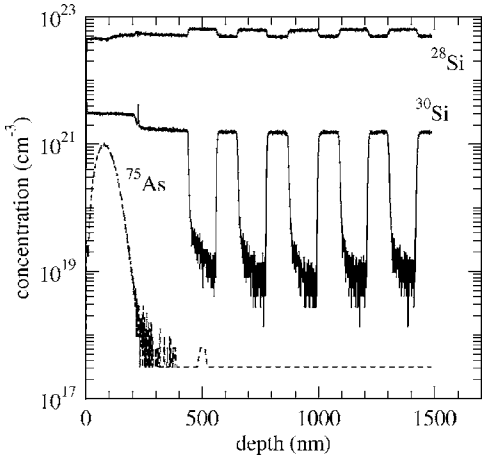

FIG. 1. SIMS concentration profiles of ^{75}As, ^{28}Si, and ^{30}Si of the As-implanted Si isotope multilayer structure.

the Si substrate and five 120-nm-thick highly enriched ^{28}Si layers, which are separated from each other by a 120-nm-thick natural Si layer. A 200-nm-thick natural Si layer was grown on top of the structure. After the growth of the single-crystalline isotope structure a 250-nm-thick amorphous natural Si layer was deposited by means of low-temperature molecular-beam epitaxy. B^+ was implanted at a dose of 7×10^{15} cm^{-2} at 32 keV and 1×10^{16} cm^{-2} at 37 keV. A heavily doped As diffusion source was prepared by sequential implants of As^+ at 130 keV with a dose of 0.7×10^{16} cm^{-2} and 1×10^{16} cm^{-2} at 160 keV into the amorphous cap layer. A P diffusion source was created by P^+ implantation at 65 and 75 keV each at 7×10^{15} cm^{-2}. Under these implantation conditions the dopants reside in the amorphous cap layer and the implantation damage is mainly generated in the amorphous layer and not in the crystalline isotope structure. Another piece of the isotope structure was implanted with Si ions at 50 and 65 keV with doses of 7×10^{15} cm^{-2} and 1×10^{16} cm^{-2}, respectively. The dopant and Si concentration profiles of the As-implanted isotope structure prior to annealing are illustrated in Fig. 1. The profiles of the B- and P-implanted isotope structures look similar. After implantation, samples of 4×4 mm^2 in dimension were sealed under argon in silica ampoules and annealed in a resistance-heated furnace at appropriate temperatures and times. Annealing of the P-implanted samples causes a root-mean-square (rms) surface roughness of approximately 100 nm, which was determined by means of atomic-force microscopy. Since this surface roughness would considerably limit the depth resolution of the diffusion profiles measured by means of secondary-ion-mass spectrometry (SIMS), all P-diffused samples were polished to a rms surface roughness of 10 nm or less. The mechanical polishing was performed on a Logitech PM5 polishing machine using Syton HT50 colloidal silica as the slurry on a MD-Chem cloth polishing pad.[5] This surface treatment improved the depth resolution by almost two orders of magnitude. No surface degradation was observed after annealing of the B- and As-implanted samples. The distribution of the dopants (B, As, or P) and self-atom (^{30}Si) were recorded with SIMS on an ATOMIKA 4500. More details about the sample preparation for the diffusion anneals and SIMS profiling are given in Refs. 5–9.

The Si-implanted sample was used to simulate the impact of ion implantation in the amorphous cap layer on Si self-diffusion in the underlying crystalline isotope structures. Several diffusion anneals were performed at temperatures and times similar to those used for the dopant-diffusion experiments. All ^{30}Si profiles obtained after annealing reveal a homogeneous broadening of the entire isotope structure.[7] The broadening is accurately described with our former results of self-diffusion under intrinsic and thermal-equilibrium conditions.[10–12] This demonstrates that ion implantation into the amorphous cap layer and even the recrystallization of the cap layer during annealing does not cause any significant transient enhanced diffusion. Obviously the excess defects created by ion implantation are effectively absorbed within the amorphous top layer and do not lead to excess native-defect concentrations in the under lying crystalline layers.

III. DIFFUSION PROFILES

Concentration profiles of ^{11}B, ^{75}As, and ^{31}P along with the corresponding ^{30}Si profiles measured with SIMS after diffusion annealing are shown in Figs. 2–4, respectively. Figure 2 shows that the Si profile associated with the in-diffusion of B reveals a faster Si diffusion for high B concentrations close to the amorphous (crystalline) interface than at the B diffusion front. A comparison of the Si profile obtained by in-diffusion of B with that expected for intrinsic and thermal-equilibrium conditions reveals a slightly higher Si diffusivity under B in-diffusion even at the deepest ^{28}Si/^{nat}Si interface [see Fig. 2(d)].

Si profiles obtained by As diffusion show an enhanced Si diffusion within the topmost isotope layers. Here the As doping concentration exceeds the intrinsic-carrier concentration. The Si profile at the deepest interface is accurately described with the diffusion coefficient for intrinsic and thermal-equilibrium conditions [see Fig. 3(d)].

Si profiles associated with the diffusion of P also indicate an enhanced interdiffusion of the topmost natural and isotopically enriched layers [see Fig. 4(d)]. The diffusion of Si at the deepest ^{28}Si/^{nat}Si interface is described with a diffusion coefficient that is close to the value determined for intrinsic and thermal-equilibrium conditions. This is a surprising result because the pronounced tail of P profiles, which are clearly at variance with the box-shaped As profiles, are generally argued to be due to a supersaturation of Si self-interstitials.[4,13] The broadening of the Si profiles demonstrates that the supersaturation of self-interstitials due to P diffusion is significantly lower than generally expected.

The concentration profiles of P and Si within the topmost ion-implanted amorphous Si layer are missing in Fig. 4 because this layer was removed prior to SIMS profiling. This had little effect on the P profile as demonstrated by Fig. 4(c), which shows the P profiles before and after removing the cap layer.

The depth-dependent broadening of the Si isotope structure observed after dopant diffusion is caused by the following: (i) The formation of charged-point defects depends on

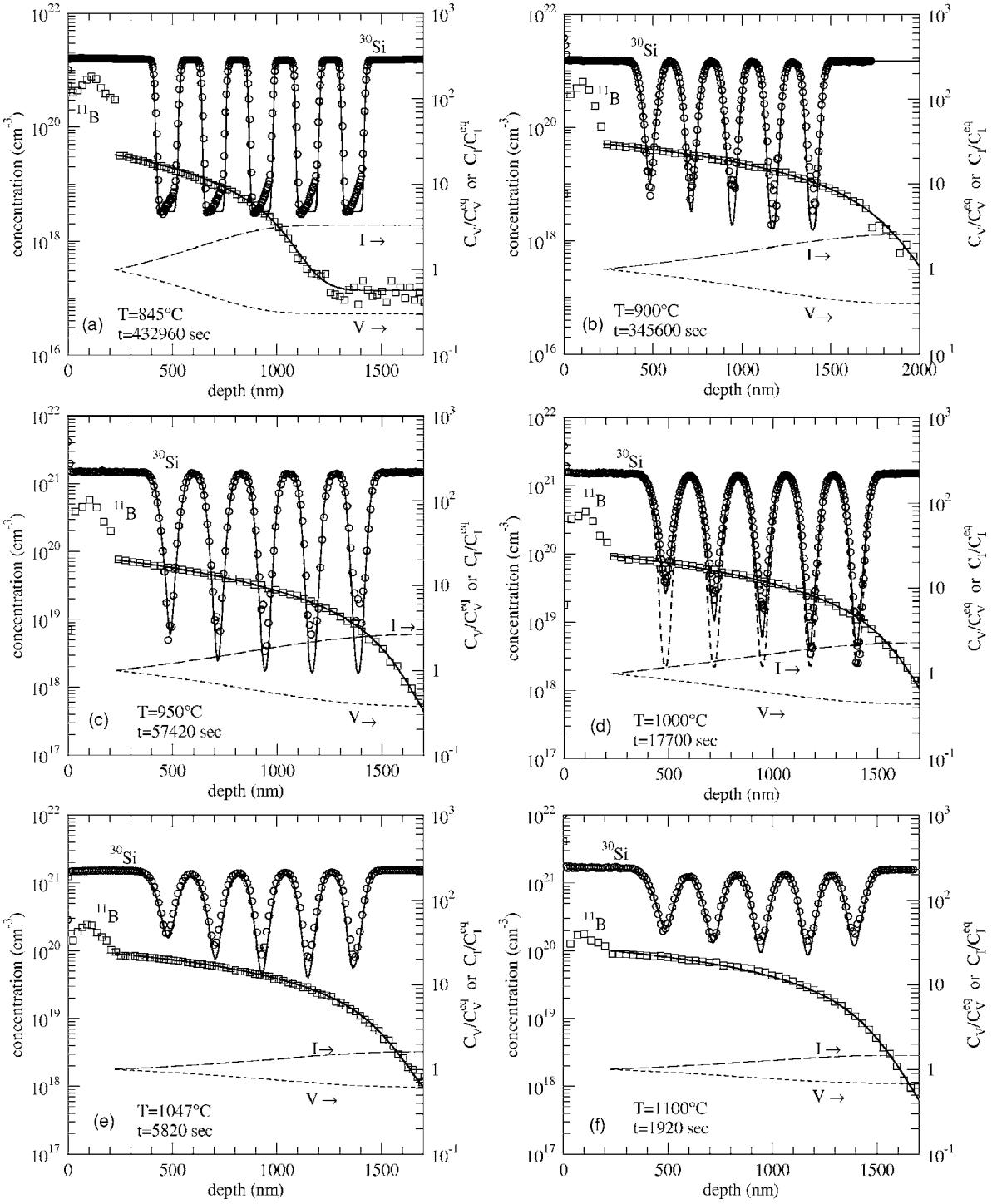

FIG. 2. SIMS concentration profiles of ^{11}B and ^{30}Si after annealing of the B-implanted isotope structure at the temperatures and times indicated in the figures. A reduced number of data points are shown for clarity. The solid lines in (a)–(f) represent best fits on the basis of reactions (1) and (2). The lower dashed lines show the corresponding calculated super- and undersaturation of self-interstitials and vacancies, respectively, which refer to the right ordinate. The upper dashed line in (d) illustrates the Si profile that is expected in the case when Si diffusion proceeds under electronically intrinsic ($n=p=n_{in}$) and thermal-equilibrium conditions ($C_{V,I}=C_{V,I}^{eq}$).

the position of the Fermi level (see Part I). As a consequence the thermal-equilibrium concentration of charged-native-point defects is altered by doping and therewith the self-diffusion coefficient. (ii) Dopant diffusion can lead to concentrations of native-point defects, which deviate from thermal equilibrium. This, in particular, holds for the native-defect-controlled mode of dopant diffusion (see Part I). (iii) *AV* and *AI* pairs between the dopant A and the vacancy and self-interstitial can contribute to Si self-diffusion [see Eq. (74) in Part I]. Whether such pairs contribute significantly to self-diffusion depends on the magnitude of the transport coefficients $C_{AV}^{eq}D_{AV}$ and $C_{AI}^{eq}D_{AI}$ compared to those of the na-

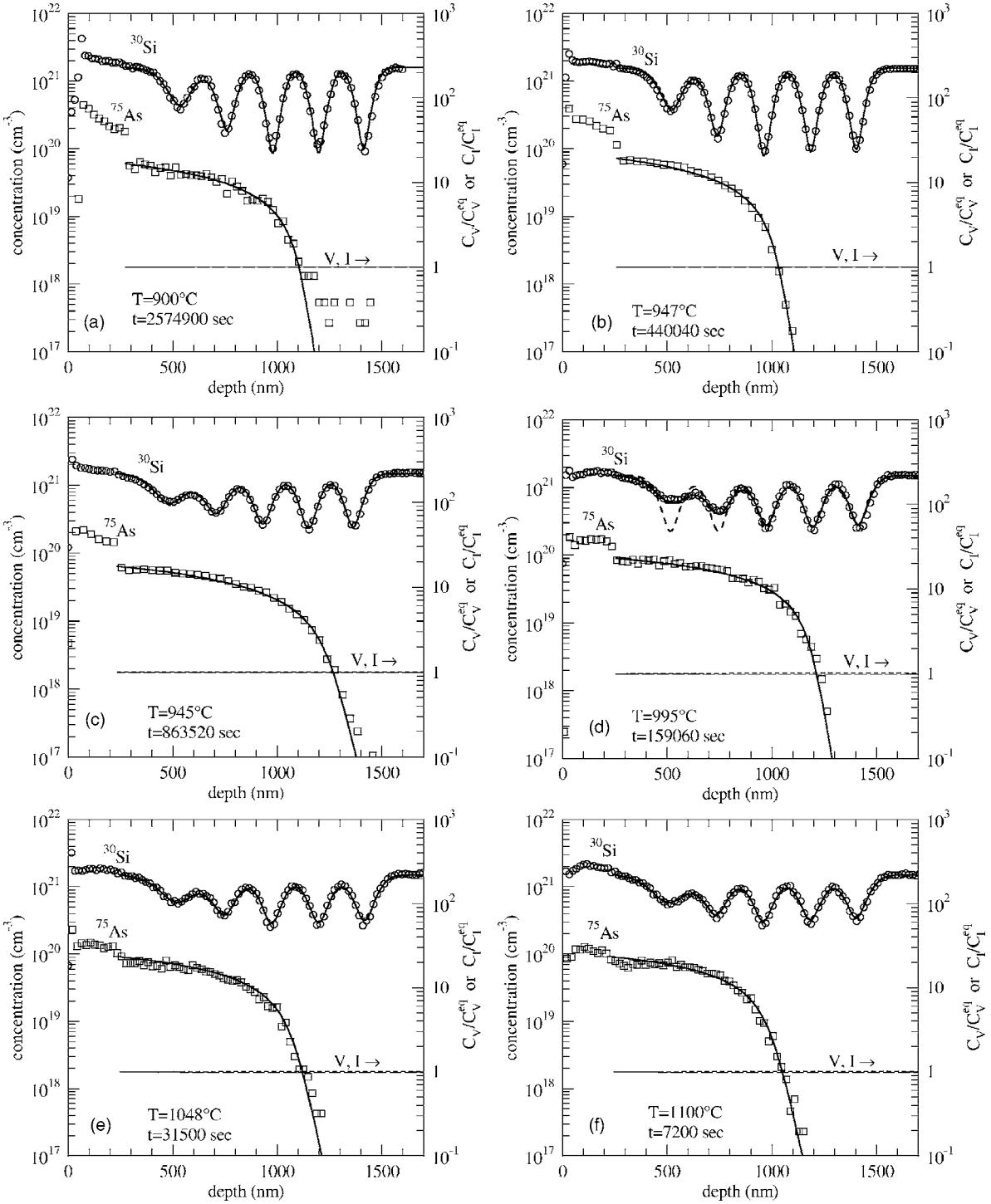

FIG. 3. SIMS concentration profiles of ^{75}As and ^{30}Si after annealing of the As-implanted Si isotope structure at the temperatures and times indicated in the figures. A reduced number of data points are shown for clarity. The solid lines in (a)–(f) represent best fits based on the reactions (3)–(6). The lower dashed lines show the corresponding normalized concentrations of self-interstitials and vacancies. The concentration of these native defects is close to the thermal-equilibrium value, i.e., $C_I/C_I^{eq} \approx 1$ and $C_V/C_V^{eq} \approx 1$. The upper dashed line in (d) shows the Si profile that is expected in the case when Si diffusion proceeds under intrinsic and thermal-equilibrium conditions.

tive defects and on the correlation factors for self-diffusion via *AV* and *AI*. In order to determine the significance of (i)–(iii) for the simultaneous diffusion of self- and dopant atoms, the profiles shown in Figs. 2–4 were analyzed on the basis of a continuum theoretical approach that takes into account appropriate diffusion-reaction equations. Details of the mathematical description are given in Part I. In the following the mechanisms that were used for modeling are presented.

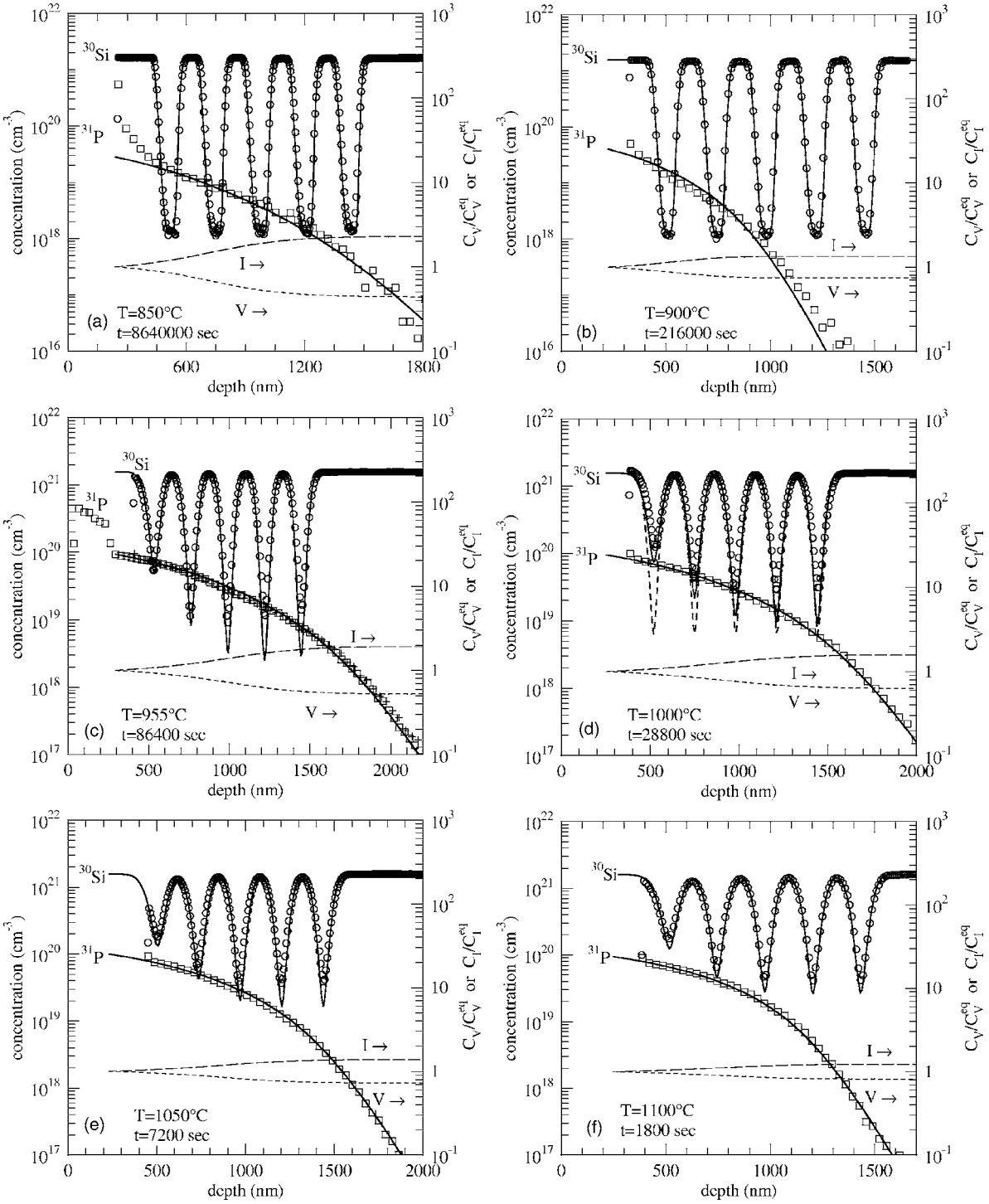

FIG. 4. SIMS concentration profiles of ^{31}P and ^{30}Si after annealing of the P-implanted Si isotope structure at temperatures and times indicated in the figures. A reduced number of data points are shown for clarity. The solid lines in (a)–(f) represent best fits on the basis of the reactions (7)–(10). The lower dashed lines show the corresponding super- and undersaturation of self-interstitials and vacancies, respectively. The upper dashed line in (d) is the Si profile that is expected in the case Si diffusion proceeds under intrinsic and thermal-equilibrium conditions. (c) shows a comparison between the P profile measured before (□) and after (+) removing the top amorphous layer.

IV. MECHANISMS OF DOPANT DIFFUSION IN SILICON

A. Diffusion of boron

The diffusion of B in Si is known to be enhanced by the injection of self-interstitials (I) (Refs. 14 and 15) and retarded by a vacancy (V) injection.[16,17] These experiments reveal that B mainly diffuses via B interstitials (B_i) or BI pairs rather than via BV pairs.[18] The in-diffusion of B at high boundary concentrations of electrically active substitutional B_s is known to create an I supersaturation.[4] Isoconcentration-

diffusion experiments showed that the B diffusivity is proportional to B concentration.[19] Such diffusion studies reflect the diffusivity for the foreign-atom-controlled mode of B diffusion because the tagged dopant diffuses under constant dopant and native-defect concentrations (see Part I). The observed linear dependence of B diffusion on the acceptor concentration tells that the charge difference between B_s and B_i is one (see the right side of Table I in Part I). Since B_s is certainly singly negatively charged, B_i must be neutral.

The interstitialcy and kick-out mechanisms are generally considered for modeling B diffusion in Si (see reactions (2) and (3) in Part I). Both mechanisms are mathematically equivalent, i.e., they predict identical diffusion profiles for local equilibrium conditions. Cowern *et al.*[20] provided experimental evidence in favor of the kick-out mechanism, which was confirmed by *ab initio* calculations of Zhu *et al.*,[21] but recent theoretical studies show that B diffuses more likely by an interstitialcy mechanism.[22–25]

For modeling the simultaneous diffusion of B and Si we consider the kick-out and dissociative mechanisms

$$B_i^0 \rightleftharpoons B_s^- + I^u + (1-u)h, \tag{1}$$

$$B_i^0 + V^k \rightleftharpoons B_s^- + (1+k)h, \tag{2}$$

with charge states u and k for I and V, respectively. Neutral (I^0), singly and doubly positively (I^+, I^{2+}), and singly negatively charged self-interstitials (I^-) were taken into account for the simulations. The dissociative mechanism (2) assures local equilibrium between I and V after sufficient long times. The charge states assumed for the vacancy are neutral (V^0), singly positive (V^+), and singly and doubly negative (V^-, V^{2-}). Note, reaction (2) is not at variance with the results of B diffusion under nonequilibrium conditions. In accord with the experimental observations reported in the literature,[14–17] reaction (2) leads to an enhanced (retarded) B diffusion for $I(V)$ injection because the residence time of B on interstitial sites increases (decreases).

B. Diffusion of arsenic

The diffusion of As in Si under intrinsic conditions is known to be enhanced under both V and I injection.[3,17] This indicates that both the interstitialcy or kick-out mechanism and the vacancy mechanism contribute to As diffusion. Isoconcentration studies revealed an As diffusion coefficient that is almost proportional to the As concentration.[26] Since the diffusion coefficient for isoconcentration conditions reflects the effective As diffusivity $D^{\mathrm{eff}}_{\mathrm{As}_s^+}$ for the foreign-atom-controlled mode, the linear-concentration dependence of $D^{\mathrm{eff}}_{\mathrm{As}_s^+}$ shows that the charge difference between As_s^+ and the mobile dopant defect is one (see Table I of Part I). This linear-concentration dependence of $D^{\mathrm{eff}}_{\mathrm{As}_s^+}$ also becomes apparent in the box-shaped profiles obtained after extrinsic diffusion of As in Si (see Fig. 3). This shape is expected for the foreign-atom-controlled mode of As diffusion via a reaction similar to the vacancy mechanism (see Table I in Part I) in the case when the substitutional dopant is singly positively charged and the mobile dopant-defect pair is neutral. The similarity between extrinsic diffusion of As in Si with high As background concentrations and extrinsic As diffusion in intrinsic Si demonstrates that As diffusion proceeds in thermal equilibrium, i.e., no super- or undersaturations of native-point defects are formed.

For modeling simultaneous As and Si diffusion we take into account the vacancy and interstitialcy mechanisms and the dopant-defect pair-assisted mechanisms of $I-V$ recombination,

$$\mathrm{As}V^j \rightleftharpoons \mathrm{As}_s^+ + V^k + (1+k-j)e^-, \tag{3}$$

$$\mathrm{As}I^0 \rightleftharpoons \mathrm{As}_s^+ + I^u + (1+u)e^-, \tag{4}$$

$$\mathrm{As}V^j + I^u \rightleftharpoons \mathrm{As}_s^+ + (1-j-u)e^-, \tag{5}$$

$$\mathrm{As}I^0 + V^k \rightleftharpoons \mathrm{As}_s^+ + (1-k)e^-. \tag{6}$$

Various charge states for $V(\in\{V^+, V^0, V^-, V^{2-}\}$ and $I(\in\{I^{2+}, I^+, I^0, I^-\})$ were assumed as well as neutral and singly negatively charged dopant-vacancy pairs $\mathrm{As}V^0$ and $\mathrm{As}V^-$. The contribution of $\mathrm{As}V^-$ to As diffusion accounts for an effective As diffusivity, which is proportional to the square of the As concentration $C_{\mathrm{As}_s^+}$ (see Table I in Part I). Assuming both neutral and singly negatively charged dopant-vacancy pairs better fits to the experimental As profiles are obtained than in the case when only $\mathrm{As}V^0$ pairs are considered. The sum of the $\mathrm{As}V^0$ and $\mathrm{As}V^-$ contributions to As diffusion determined from our simulations are in close agreement with the As diffusion coefficient under isoconcentration conditions[26] (see Sec. VI). This demonstrates that the apparent almost-linear-concentration dependence of As diffusion actually consists of a linear- and quadratic-concentration dependence.

The interstitialcy mechanism (4) and dopant-defect pair-assisted recombination (6) of V^k were considered to mediate As diffusion instead of the mathematically equivalent kick-out and dissociative mechanisms with mobile interstitials As_i^0 [see reactions (3) and (4) in Part I). This assignment is arbitrary and not yet established but is preferred here because it reflects the larger size of As atoms compared to B and P atoms, which makes it more likely to form AsI pairs than interstitial As_i.

In order to consider the experimental observation that As diffusion is similarly enhanced under both V and I injection, the contributions of the interstitialcy and vacancy mechanisms to As diffusion under intrinsic conditions are set equally. In the nomenclature often used in the literature (see, e.g., Ref. 4), this means that the fractional interstitialcy component of As diffusion is 0.5 or, in the term described in Part I, the reduced diffusion coefficient $D^*_{\mathrm{As}I^0}$ of neutral $\mathrm{As}I^0$ pairs equals $D^*_{\mathrm{As}V^0}$ of neutral $\mathrm{As}V^0$ pairs.

In contrast to Uematsu *et al.*,[4] a reaction which gives rise to a deactivation of substitutional As was not taken into account because the As profiles illustrated in Fig. 3 all exhibit As concentrations below or close to 10^{20} cm^{-3}. At this doping level significant deactivation of As is not expected.

C. Diffusion of phosphorus

Intrinsic diffusion of P in Si has been demonstrated to be retarded under nitridation.[16,17] Nitridation of a bare Si surface causes an injection of vacancies leading to a V supersaturation. From the degree of the retardation it was concluded that the intrinsic diffusion of P is mainly mediated by PI pairs or interstitial phosphorus P_i.[27] Accordingly the fractional interstitialcy or interstitial component of intrinsic P diffusion is close to unity. For extrinsic P doping the retardation of P diffusion under nitridation decreases,[17] which indicates an increased contribution of vacancies to P diffusion. The P diffusivity was found to be proportional to the square of the P concentration for very high doping levels.[28] Therefore, Uematsu[4] assumed that the vacancy mechanism with singly negatively charged dopant-vacancy pairs PV^- and V^{2-} dominates P diffusion for very high doping levels. For lower doping levels isoconcentration studies of Makris and Masters[29] showed that the P diffusivity increases approximately linear with the free-electron concentration. Hence, like in the case of As, the charge difference between P_s^- and the PI pair or the interstitial P_i must be one. In accord with the work of Uematsu,[4] we assume neutral P_i^0 and negatively charged PV^- pairs for the simulation of P diffusion. In addition we take into account singly positively charged P_i^+. This defect is required to accurately describe both P and Si diffusion profiles. Based on the results of the above-mentioned P diffusion studies and the requirement to describe the simultaneous diffusion of P and Si, the following reactions were considered for the simulation of P diffusion in the Si isotope structures:

$$PV^- \rightleftharpoons P_s^+ + V^k + (2+k)e^-, \tag{7}$$

$$PV^- + I^u \rightleftharpoons P_s^+ + (2-u)e^-, \tag{8}$$

$$P_i^q \rightleftharpoons P_s^+ + I^u + (1+u-q)e^-, \tag{9}$$

$$P_i^q + V^k \rightleftharpoons P_s^+ + (1-k-q)e^-, \tag{10}$$

where P_i^q is assumed to exist as a neutral and singly positively charged defect. For V^k and I^u we used the same charge states as those in reactions (1)–(6) for modeling B and As diffusion.

D. Modeling of dopant and self-diffusion

Based on reactions (1)–(10) the partial-differential equations for each point defect involved in the defect reactions were set up according to the details given in Part I. Since several reactions can contribute to the formation (annihilation) of a point defect, several reaction terms enter the partial-differential equations. The model parameters of the normalized-differential-equation system are the reduced-diffusion coefficients $D_X^* = C_X^{eq} D_X / C_{A_s^m}^{eq}$ and reduced-equilibrium concentrations $C_X^{eq} / C_{A_s^m}^{eq}$ with $X \in \{A_i^q, AI^v, AV^j, V^k, I^u\}$ where A represents the dopants B, As, and P. The reaction constants were chosen sufficiently high such that local equilibrium is established for the times realized in the experiments. The successful simulation of the experimental profiles justifies *ex post* this approach. The initial and boundary conditions considered for the numerical solution of the equation system are described in Sec. III C of Part I.

The thermal-equilibrium concentrations of native-point defects in Si are below the detection limit of state-of-the-art analyses techniques such as positron annihilation spectroscopy and dilatometer measurements. The total concentrations of V and I in thermal equilibrium were calculated from

$$C_I^{eq} = 2.9 \times 10^{24} \exp\left(-\frac{3.18\ \text{eV}}{k_B T}\right)\ \text{cm}^{-3}, \tag{11}$$

$$C_V^{eq} = 1.4 \times 10^{24} \exp\left(-\frac{2.44\ \text{eV}}{k_B T}\right)\ \text{cm}^{-3}. \tag{12}$$

The temperature dependence of C_I^{eq} follows from the analysis of Zn diffusion experiments in Si, which were performed at temperatures between 870 and 1208 °C.[30] The equation represents a definitive upper bound for C_I^{eq}. The expression for C_V^{eq} comprises data from radiation enhanced Si self-diffusion[31] and Ir diffusion in Si (Refs. 32 and 33) for 780–1200 °C. Taking into account Eqs. (11) and (12) and a concentration of substitutionally dissolved foreign atoms of 10^{20} cm^{-3}, which is similar to the maximum-dopant concentrations observed in this work, the reduced-equilibrium concentration of V is about 10^{-5}. Assuming the relationship $C_V^{eq} = 10^{15} \exp(-4.5\text{eV}/k_B T)$ deduced from the simulation of crystal growth and defect formation during wafer processing,[34] even lower values are obtained for the reduced V concentration. Equation (11) with $C_{A_s^m}^{eq} = 10^{20}$ cm^{-3} yields $C_I^{eq} / C_{A_s^m}^{eq} \approx 10^{-7}$ for the reduced-equilibrium concentration of self-interstitials. The equilibrium concentrations of the mobile species A_i^q, AI^v, and AV^j are assumed to be four to three orders of magnitude lower than $C_{A_s^m}^{eq}$. This is a reasonable assumption for mainly substitutionally dissolved foreign atoms. The simulations performed with these settings for $C_X^{eq} / C_{A_s^m}^{eq}$ are fairly insensitive to the reduced-equilibrium concentrations, i.e., orders-of-magnitude lower or higher values do not significantly affect the simulations. This shows that the dopant and Si profiles are mainly sensitive to the reduced-diffusion coefficients $D_X^* = C_X^{eq} D_X / C_{A_s^m}^{eq}$.

E. Fitting of experimental profiles

The model parameter $D_{X^0}^*$ of the neutral-point defects and the energy levels of the defects were adjusted to reproduce the experimental profiles. Based on $D_{X^0}^*$ the reduced-diffusion coefficients of the corresponding charged defects were calculated by means of the equations given in Sec. III A of Part I. For the temperature dependence of the Fermi level E_f^{in} under intrinsic conditions we used the expressions given by Thurmond.[35] For the calculation of D_X^* we assumed that the diffusion coefficients of X are similar for the various charge states, i.e., $D_{X^0} \approx D_{X^{i\pm}}$ and that the degeneracy factors g are equal one. It is noted that the assumption $D_{X^0} \approx D_{X^{i\pm}}$ does not limit the accuracy of D_X^*. This complies with the

fact that the experimental profiles are mainly sensitive to $D_X^*=C_X^{eq}D_X/C_{A_s^m}^{eq}$ rather than to $C_X^{eq}/C_{A_s^m}^{eq}$. In this respect, the energy levels determined for X are less accurate than the transport capacities $C_X^{eq}D_X$.

The setting of the reduced-diffusion coefficients D_X^* via the model parameter $D_{X^0}^*$ and the energy levels of X is advantageous because it enables diffusion simulations of all dopants on the basis of the same native-point-defect parameters. In previous simulations we attempted to determine the properties of native-point defects from separate analyses of B, As, and P diffusion in Si isotope structures. However, we did not obtain overall consistent values for the transport capacities $C_X^{eq}D_X$. In particular, it was difficult to determine whether or not singly negatively charged self-interstitials I^- contribute to self-diffusion under n-type doping conditions.[9]

The self-diffusion coefficient D_{Si} is given by the sum of the contributions of charged vacancies and self-interstitials to self-diffusion. Under thermal equilibrium the self-diffusion coefficient is given by

$$D_{Si}^{eq}=\left(\sum_k f_{V^k}C_{V^k}^{eq}D_{V^k}+\sum_u f_{I^u}C_{I^u}^{eq}D_{I^u}\right)\frac{1}{C_o}, \tag{13}$$

with $V\in\{V^+,V^0,V^-,V^{2-}\}$ and $I\in\{I^{2+},I^+,I^0,I^-\}$. $C_o(=5\times10^{22}\ \mathrm{cm}^{-3})$ and f_{V^k,I^u} are the Si atom density and diffusion-correlation factors, respectively. The correlation factor for self-diffusion via vacancies in a diamond structure is 0.5 for all charge states.[36] In the case of the self-interstitial the charge state strongly affects its configurations.[37] Accordingly, also the diffusion-correlation factor of self-interstitials can be different for each charge state. However, calculations of correlation factors for different configurations of self-interstitials are lacking. Therefore, for simplicity we assume the same factor for all charge states. We considered the value of 0.73 reported by Compaan and Haven[38] and 0.56 calculated by Posselt *et al.*[39,40] by means of molecular dynamic simulations. $f_I=0.73$ corresponds to the correlated diffusion of a tetrahedral self-interstitial. The value reported by Posselt *et al.* was obtained for the migration of a split interstitial. According to theoretical calculations this split interstitial is the most stable defect among the various possible self-interstitial configurations.[39,41–43] Therefore we used $f_I=0.56$ for modeling Si self-diffusion. On the basis of this value an activation enthalpy of self-diffusion via vacancies is obtained that is consistent with the activation enthalpies determined for vacancy-mediated dopant diffusion (see Sec. VI).

The self-diffusion coefficient D_{Si}^{eq} of Si for intrinsic and thermal-equilibrium conditions was recently determined to

$$D_{Si}^{eq}=560\exp\left(-\frac{4.76\ \mathrm{eV}}{k_BT}\right)\ \mathrm{cm}^2\ \mathrm{s}^{-1} \tag{14}$$

for temperatures between 855 and 1388 °C.[10–12] In order to make an allowance for this result all simulations of dopant diffusion were performed under the constraint that the sum of the relative intrinsic contributions of native-point defects to self-diffusion adds up to D_{Si}^{eq}. Additionally, we consider that the sum of the intrinsic contributions of charged self-interstitials to self-diffusion equals the total self-interstitial contribution. This contribution is known from Zn diffusion in Si and is given by[30]

$$\frac{1}{C_o}C_I^{eq}D_I=2980\exp\left(-\frac{4.95\ \mathrm{eV}}{k_BT}\right)\ \mathrm{cm}^2\ \mathrm{s}^{-1} \tag{15}$$

for temperatures between 870 and 1208 °C. With Eqs. (14) and (15) the intrinsic V contribution to self-diffusion is obtained via

$$\frac{1}{C_o}C_V^{eq}D_V=\frac{1}{f_V}\left(D_{Si}^{eq}-\frac{1}{C_o}f_IC_I^{eq}D_I\right), \tag{16}$$

taking into account $f_{V^k}=0.5$ and the values calculated for f_{I^u}. Assuming $f_I=0.73$ for all charge states, the V contribution to self-diffusion for intrinsic conditions is

$$\frac{1}{C_\circ}C_V^{eq}D_V=6.2\exp\left(-\frac{4.33\ \mathrm{eV}}{k_BT}\right)\ \mathrm{cm}^2\ \mathrm{s}^{-1}, \tag{17}$$

and for $f_I=0.56$ we obtain

$$\frac{1}{C_\circ}C_V^{eq}D_V=43\exp\left(-\frac{4.56\ \mathrm{eV}}{k_BT}\right)\ \mathrm{cm}^2\ \mathrm{s}^{-1}. \tag{18}$$

For the simulation of the simultaneous self- and dopant diffusion the relative contributions of charged native-point defects to self-diffusion for intrinsic conditions were calculated on the basis of Eqs. (14), (15), and (18) by means of the equations given in Sec. III A of Part I. The relative contributions were referred to extrinsic doping conditions and multiplied by the ratio $C_o/C_{As^m}^{eq}$ in order to set the values for the model parameters $D_X^*(X\in\{V^+,V^0,V^-,V^{2-},I^{2+},I^+,I^0,I^-\})$. $D_{B_i^0}^*$, $D_{AsV^0}^*$, $D_{P_i^0}^*$, and $D_{PV^-}^*$ were directly adjustable parameters whereas D_X^* of charged native defects, $D_{P_i^+}^*$, and $D_{AsV^-}^*$ were modified via the energy levels of X, $E_{P_i^+}$ and E_{AsV^-}, respectively. The parameter $D_{AsI^0}^*$ was set equal to $D_{AsV^0}^*$ in accord with previous results (see Sec. IV B). Altogether, 12 adjustable parameters, which consist of eight energy levels and four reduced-diffusion coefficients remain for the simulation of the simultaneous self- and dopant diffusion in Si isotope structures under the constraints that Eqs. (14) and (15) hold.

V. RESULTS

The solid lines in Figs. 2–4 are best fits of the experimental profiles, which were obtained on the basis of the above-mentioned reactions and the constraints for the model parameters. The self-diffusion profiles associated with the B, As, and P profiles were calculated with $f_V=0.5$ and $f_I=0.56$. The long- and short-dashed lines are the corresponding normalized concentrations of I and V, respectively. Both extrinsic B and P diffusion result in an I supersaturation and V undersaturation. On the other hand, extrinsic As diffusion proceeds under thermal equilibrium of I and V. The simultaneous diffusion of dopants and self-atoms and the different diffusion modes established by the n- and p-type dopants lead to profiles that are sensitive to the properties of native-point defects.

The *p*-type dopant B and its diffusion in the isotope multilayer structure favors the formation of positively charged self-interstitials whose contribution to self-diffusion decreases along the B profile due to the gradual change of the doping level. The *I* supersaturation causes a *V* undersaturation and as a consequence suppresses the diffusion of B via the dissociative mechanism (2). Accordingly, the B and Si profiles are mainly sensitive to the model parameters $D^*_{I^0}$, $D^*_{I^+}$, $D^*_{I^{2+}}$, and $D^*_{B^0_i}$.

The diffusion of As proceeds in the foreign-atom-controlled mode. Hence the self-diffusion is only affected by the *n*-type dopant via the Fermi-level effect. The enhanced self-diffusion in the region of high As concentration demonstrates that negatively charged native defects exist. However, the experiments do not reveal the nature of these defects. In this respect, the As and Si profiles are mainly sensitive to $D^*_{AsV^0}(=D^*_{AsI^0})$ and $D^*_{AsV^-}$ and the reduced-diffusion coefficients of not yet specified negatively charged native defects.

The diffusion of P in the isotope structure leads to an *I* supersaturation and *V* undersaturation and therewith suppresses the contribution of vacancies in P and Si diffusion compared to the diffusion of As. This increases the sensitivity of the P and Si profiles to negatively charged self-interstitials. The demand to describe the diffusion of all dopants and the corresponding Si profiles at a given temperature with the same energy levels of the native-point defects led to the conclusion that negatively charged vacancies rather than negatively charged self-interstitials dominate under *n*-type doping. Successful modeling of the simultaneous P and Si diffusion requires a contribution of singly positively charged mobile P defects to P diffusion. Generally, the extended tail of the P profiles compared to the much steeper As profile at the diffusion front is explained with the *I* supersaturation created during P diffusion. Our experiments show that this interpretation is not fully correct. The supersaturation that would be required to explain the extended P profile predicts an enhanced self-diffusion in the tail region that is not confirmed by the experiments. In order to account for the extended tail, a mobile P species must be assumed whose effective diffusivity is concentration independent. According to Part I, the charge difference between substitutional P^+_s and the unknown mobile P must be zero. Therefore we propose that a singly positively interstitial P^+_i is involved in reactions (9) and (10).

In addition to the dopant and Si profiles illustrated in Figs. 2–4 also diffusion profiles of B, As, and P given in the literature are fully described on the basis of reactions (1)–(10) and the above-mentioned constraints for the model parameters (see Figs. 5–7). Uematsu[4] considered in his analysis of As diffusion also a deactivation of As^+_s in order to explain the difference between the electrical active and total As concentration in the profiles measured by Murota *et al.*[47,48] This work shows that the concentration profiles of electrically active As can be accurately described on the basis of reactions (3)–(6) with model parameters that are in good agreement with the results of the simultaneous As and Si diffusion. Obviously, the deactivation does not significantly affect the profile of electrically active As.

The simulations of the dopant and Si profiles illustrated in Figs. 2–7 yield the reduced-diffusion coefficients of the dopants. The data are referred to intrinsic conditions by means of Eq. (72) given in Part I. The total intrinsic-dopant-diffusion coefficient is equal to the sum of the reduced-intrinsic-diffusion coefficients of the various mobile dopant species [see Eq. (18) of Part I]. In the case of B diffusion only the mobile defect B^0_i contributes whereas the mobile dopant-defect pairs AsV^0, AsI^0, and AsV^- contribute to As diffusion. On the other hand, P diffusion proceeds by means of P^0_i, P^+_i, and PV^-. Therefore, the total intrinsic diffusivities of B, As, and P consist of the following contributions:

$$D_B(n_{in}) = D^*_{B^0_i}(n_{in}), \tag{19}$$

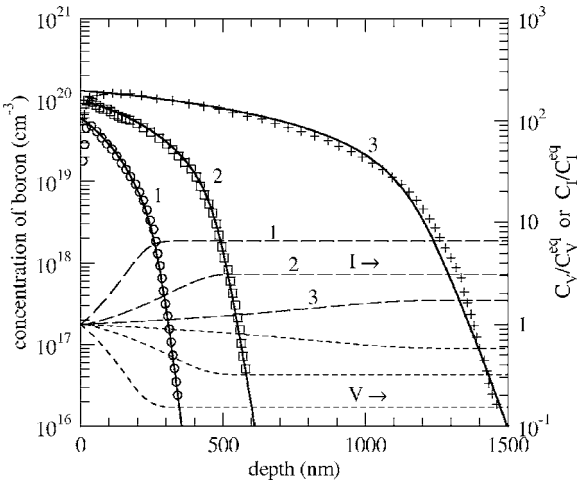

FIG. 5. SIMS concentration profiles of ^{11}B measured by Arienzo *et al.* (Ref. 46) after annealing at (1) 850 °C for 14 400 s (○), (2) 950 °C for 3600 s (□), and (3) 1050 °C for 3600 sec (+). The solid lines represent best fits on the basis of reactions (1) and (2). The long- and short-dashed lines show the corresponding calculated super- and undersaturation of self-interstitials and vacancies, respectively.

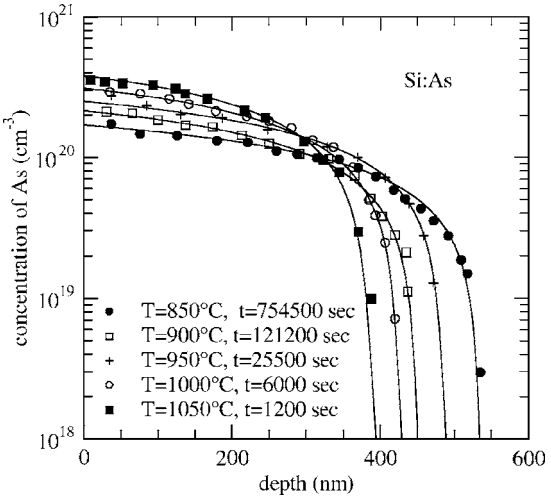

FIG. 6. Concentration profiles of electrically active ^{75}As measured by Murota *et al.* (Refs. 47 and 48) after annealing at the temperatures and times indicated. The solid lines represent best fits on the basis of reactions (3)–(6). The corresponding calculated concentrations of *I* and *V* are in thermal equilibrium, i.e., $C_{V,I}=C^{eq}_{V,I}$ and are omitted for clarity.

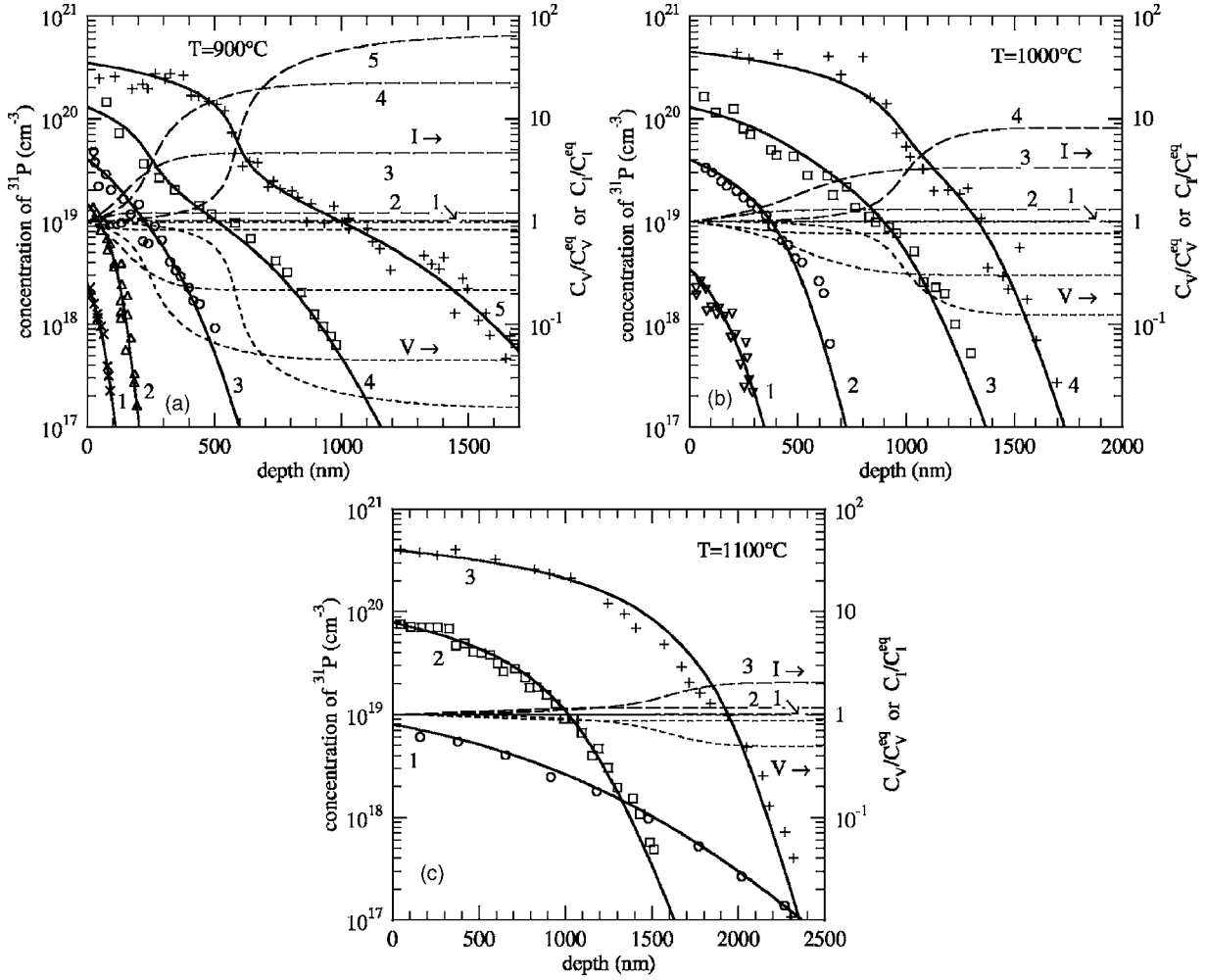

FIG. 7. Concentration profiles of electrically active ^{31}P measured by Yoshida *et al.* (Refs. 49 and 50) after annealing at (a) 900 °C for 14 400 s, (b) 1000 °C for 3600 s (+) and 7200 s (□, ○, △), and (c) 1100 °C for 1500 s (+), 3600 s (□) and 28 800 s (○). The solid lines represent best fits on the basis of reactions (7)–(10). The long- and short-dashed lines show the corresponding super- and undersaturation of self-interstitials and vacancies, respectively.

$$D_{\mathrm{As}}(n_{\mathrm{in}}) = D^*_{\mathrm{As}V^0}(n_{\mathrm{in}}) + D^*_{\mathrm{As}I^0}(n_{\mathrm{in}}) + D^*_{\mathrm{As}V^-}(n_{\mathrm{in}}), \quad (20)$$

$$D_{\mathrm{P}}(n_{\mathrm{in}}) = D^*_{\mathrm{P}^0_i}(n_{\mathrm{in}}) + D^*_{\mathrm{P}^+_i}(n_{\mathrm{in}}) + D^*_{\mathrm{P}V^-}(n_{\mathrm{in}}). \quad (21)$$

$D^*_X(n_{\mathrm{in}})(X \in \{\mathrm{B}^0_i, \mathrm{As}V^0, \mathrm{As}V^-, \mathrm{As}I^0, \mathrm{P}^0_i, \mathrm{P}^+_i, \mathrm{P}V^-\})$ and $D_A(n_{\mathrm{in}})(A \in \{\mathrm{B}, \mathrm{As}, \mathrm{P}\})$ are summarized in Tables I–III together with the respective diffusion temperature T and time t, maximum-dopant concentration $C^{\mathrm{eq}}_{A^m_s}$, maximum-hole p^{eq} or electron n^{eq} concentrations [see Eq. (77) in Part I], and the intrinsic-carrier concentration n_{in} reported by Morin and Maita.[44]

Figure 8 shows the B, As, and P diffusion coefficients for intrinsic conditions in comparison to results given in the literature. The total intrinsic B, As, and P diffusion coefficients deduced from modeling the simultaneous self- and dopant diffusion and from modeling the dopant profiles given in the literature are described by

$$D_{\mathrm{B}} = \left(0.87^{+1.03}_{-0.47}\right)\exp\left(-\frac{(3.46 \pm 0.08)\ \mathrm{eV}}{k_B T}\right)\ \mathrm{cm}^2/\mathrm{s}, \quad (22)$$

$$D_{\mathrm{As}} = \left(47^{+35}_{-20}\right)\exp\left(-\frac{(4.20 \pm 0.06)\ \mathrm{eV}}{k_B T}\right)\ \mathrm{cm}^2/\mathrm{s}, \quad (23)$$

$$D_{\mathrm{P}} = \left(0.75^{+1.12}_{-0.45}\right)\exp\left(-\frac{(3.42 \pm 0.10)\ \mathrm{eV}}{k_B T}\right)\ \mathrm{cm}^2/\mathrm{s}, \quad (24)$$

and illustrated in Fig. 8 as solid lines. The dashed lines in Fig. 8 are the intrinsic diffusivities of B,[45] As,[26] and P (Ref. 29) reported in the literature. The preexponential factor $D_0 = 0.87\ \mathrm{cm}^2\ \mathrm{s}^{-1}$ and activation enthalpy $Q = 3.46$ eV of B diffusion are in excellent agreement with $D_0 = 0.55\ \mathrm{cm}^2\ \mathrm{s}^{-1}$ and $Q = 3.42$ eV reported by Antoniadis *et al.*[45] The Arrhenius parameters of As diffusion, $D_0 = 47\ \mathrm{cm}^2\ \mathrm{s}^{-1}$ and $Q = 4.20$ eV, are in excellent agreement with the values of D_0

TABLE I. Data of the reduced B diffusion coefficients $D^*_{B^0_i}[=D_B(n_{in})]$ for intrinsic conditions, which were determined from modeling the simultaneous diffusion of B and Si in Si isotope multilayer structures and from modeling B profiles given in the literature. Also listed are the corresponding diffusion temperature T and time t, maximum B concentration $C^{eq}_{B^-_s}$, maximum hole concentration p^{eq}, and intrinsic carrier concentration n_{in} after Morin and Maita (Ref. 44).

T (°C)	t (s)	$C^{eq}_{B^-_s}$ (cm^{-3})	p^{eq} (cm^{-3})	n_{in} (cm^{-3})	$D^*_{B^0_i}$ ($cm^2\,s^{-1}$)	Reference
845	432960	3.30×10^{19}	3.33×10^{19}	3.32×10^{18}	1.99×10^{-16}	This work
845	1036140	3.10×10^{19}	3.14×10^{19}	3.32×10^{18}	2.17×10^{-16}	This work
850	14400	6.00×10^{19}	6.02×10^{19}	3.44×10^{18}	2.92×10^{-16}	46
850	14400	4.50×10^{19}	4.53×10^{19}	3.44×10^{18}	3.65×10^{-16}	46
900	345600	5.10×10^{19}	5.15×10^{19}	4.91×10^{18}	9.55×10^{-16}	This work
950	57420	7.50×10^{19}	7.56×10^{19}	6.85×10^{18}	3.53×10^{-15}	This work
950	3600	9.50×10^{19}	9.55×10^{19}	6.85×10^{18}	5.24×10^{-15}	46
950	3600	8.50×10^{19}	8.55×10^{19}	6.85×10^{18}	5.60×10^{-15}	46
1000	17700	9.40×10^{19}	9.49×10^{19}	9.34×10^{18}	1.38×10^{-14}	This work
1047	5820	9.10×10^{19}	9.26×10^{19}	1.23×10^{18}	5.97×10^{-14}	This work
1050	3600	1.30×10^{20}	1.31×10^{20}	1.25×10^{18}	5.24×10^{-14}	46
1050	3600	1.15×10^{20}	1.16×10^{20}	1.25×10^{18}	6.45×10^{-14}	46
1100	1920	1.00×10^{20}	1.03×10^{20}	1.65×10^{18}	2.08×10^{-13}	This work

$=60\ cm^2\,s^{-1}$ and $Q=4.20$ eV given by Masters and Fairfield.[26] The data of intrinsic P diffusion are within a factor of 2 consistent with the data of Makris and Masters,[29] which follow an Arrhenius equation with $D_0=5.3\ cm^2\,s^{-1}$ and $Q=3.69$ eV. The good agreement between the total intrinsic diffusivities determined in this work with the data given in the literature confirms the reduction of the extrinsic diffusion coefficients to intrinsic conditions and the values reported by Morin and Maita[44] for the intrinsic carrier concentration.

The relative contributions to the total As and P diffusion coefficients are listed in Tables II and III, respectively. Fitting an Arrhenius equation to the results yields

$$D^*_{AsV^0}=\left(11\,^{+10}_{-5}\right)\exp\left(-\frac{(4.12\pm0.07)\ \text{eV}}{k_BT}\right)\ cm^2/s, \tag{25}$$

TABLE II. Intrinsic As diffusion coefficient D_{As} and the reduced-diffusion coefficients $D^*_{AsV^0}$, $D^*_{AsI^0}$, and $D^*_{AsV^-}$ for intrinsic conditions. Data were determined from modeling the interference between As diffusion and Si diffusion in Si isotope multilayer structures and from modeling As diffusion in natural Si. All profiles were measured by means of SIMS after diffusion annealing at the given temperatures T and times t. For the analysis of As diffusion in natural Si we considered the profiles given by Murota *et al.* (Refs. 47 and 48). $C^{eq}_{As^+_s}$, n^{eq}, and n_{in} denote the maximum As concentration, maximum electron concentration, and intrinsic carrier concentration, respectively.

T (°C)	t (s)	$C^{eq}_{As^+_s}$ (cm^{-3})	n^{eq} (cm^{-3})	n_{in} (cm^{-3})	$D^*_{AsV^0}=D^*_{AsI^0}$ ($cm^2\,s^{-1}$)	$D^*_{AsV^-}$ ($cm^2\,s^{-1}$)	D_{As} ($cm^2\,s^{-1}$)	References
850	754500	1.70×10^{20}	1.70×10^{20}	3.44×10^{18}	3.44×10^{-18}	3.38×10^{-19}	7.22×10^{-18}	47 and 48
900	2574900	6.00×10^{19}	6.04×10^{19}	4.91×10^{18}	1.95×10^{-17}	5.25×10^{-19}	3.96×10^{-17}	This work
900	121200	2.15×10^{20}	2.15×10^{20}	4.01×10^{18}	2.09×10^{-17}	1.52×10^{-18}	4.33×10^{-17}	47 and 48
945	863520	6.40×10^{19}	6.47×10^{19}	6.63×10^{18}	1.13×10^{-16}	3.16×10^{-18}	2.29×10^{-16}	This work
947	440040	7.20×10^{19}	7.26×10^{19}	6.72×10^{18}	1.11×10^{-16}	3.12×10^{-18}	2.25×10^{-16}	This work
950	25500	2.50×10^{20}	2.50×10^{20}	6.85×10^{18}	1.26×10^{-16}	1.36×10^{-17}	2.66×10^{-16}	47 and 48
995	159060	9.00×10^{19}	9.09×10^{19}	9.07×10^{18}	3.49×10^{-16}	7.65×10^{-17}	7.75×10^{-16}	This work
1000	6000	3.10×10^{20}	3.10×10^{20}	9.34×10^{18}	5.30×10^{-16}	4.29×10^{-17}	1.10×10^{-15}	47 and 48
1048	31500	9.00×10^{19}	9.17×10^{19}	1.24×10^{19}	2.09×10^{-15}	4.38×10^{-16}	4.62×10^{-15}	This work
1050	1200	3.80×10^{20}	3.80×10^{20}	1.25×10^{19}	2.47×10^{-15}	2.00×10^{-16}	5.14×10^{-15}	47 and 48
1100	7200	9.00×10^{19}	9.29×10^{19}	1.65×10^{19}	7.62×10^{-15}	4.19×10^{-15}	1.94×10^{-14}	This work

TABLE III. Intrinsic P diffusion coefficient D_P and the reduced diffusion coefficients $D^*_{P^0_i}$, $D^*_{P^+_i}$, and $D^*_{PV^-}$ for intrinsic conditions. Data were determined from modeling the interference between P and Si diffusion in Si isotope multilayer structures and from modeling P diffusion in natural Si. All profiles were measured by means of SIMS after diffusion annealing at the given temperatures T and times t. For the analysis of P diffusion in natural Si we considered the profiles given by Yoshida *et al.*[49,50]. $C^{eq}_{P^+_s}$, n^{eq}, n_{in} denote the maximum P concentration, maximum electron concentration, and intrinsic carrier concentration, respectively.

T (°C)	t (s)	$C^{eq}_{P^+_s}$ (cm^{-3})	n^{eq} (cm^{-3})	n_{in} (cm^{-3})	$D^*_{P^0_i}$ ($cm^2\ s^{-1}$)	$D^*_{P^+_i}$ ($cm^2\ s^{-1}$)	$D^*_{PV^-}$ ($cm^2\ s^{-1}$)	D_P ($cm^2\ s^{-1}$)	References
850	864000	2.80×10^{19}	2.84×10^{19}	3.44×10^{18}	3.51×10^{-17}	5.41×10^{-16}		5.76×10^{-16}	This work
900	216000	4.00×10^{19}	4.06×10^{19}	4.91×10^{18}	6.05×10^{-17}	1.12×10^{-15}		1.18×10^{-15}	This work
900	14400	3.50×10^{20}	3.50×10^{20}	4.91×10^{18}	7.86×10^{-16}	7.47×10^{-16}	6.90×10^{-18}	1.54×10^{-15}	49 and 50
900	14400	1.30×10^{20}	1.30×10^{20}	4.91×10^{18}	9.06×10^{-16}	8.61×10^{-16}	2.14×10^{-18}	1.77×10^{-15}	49 and 50
900	14400	4.00×10^{19}	4.06×10^{19}	4.91×10^{18}	1.33×10^{-15}	1.27×10^{-15}		2.60×10^{-15}	49 and 50
900	14400	1.50×10^{19}	1.65×10^{19}	4.91×10^{18}	5.97×10^{-16}	5.68×10^{-16}		1.17×10^{-15}	49 and 50
900	14400	2.50×10^{18}	6.32×10^{18}	4.91×10^{18}	4.66×10^{-16}	4.44×10^{-16}		9.16×10^{-16}	49 and 50
955	86400	9.30×10^{19}	9.35×10^{19}	7.07×10^{18}	9.83×10^{-16}	6.59×10^{-15}		7.57×10^{-15}	This work
1000	18000	9.50×10^{19}	9.59×10^{19}	9.34×10^{18}	3.31×10^{-15}	2.37×10^{-14}		2.70×10^{-14}	This work
1000	28800	9.50×10^{19}	9.59×10^{19}	9.34×10^{18}	3.31×10^{-15}	2.18×10^{-14}		2.51×10^{-14}	This work
1000	3600	4.50×10^{20}	4.50×10^{20}	9.34×10^{18}	9.55×10^{-15}	1.10×10^{-14}	1.81×10^{-16}	2.08×10^{-14}	49 and 50
1000	7200	1.30×10^{20}	1.31×10^{20}	9.34×10^{19}	1.07×10^{-14}	1.24×10^{-14}	5.11×10^{-17}	2.32×10^{-14}	49 and 50
1000	7200	4.00×10^{19}	4.21×10^{19}	9.34×10^{19}	9.99×10^{-15}	1.15×10^{-14}		2.15×10^{-14}	49 and 50
1000	7200	3.50×10^{18}	1.13×10^{19}	9.34×10^{19}	7.47×10^{-15}	8.63×10^{-15}		1.61×10^{-14}	49 and 50
1050	7200	1.00×10^{20}	1.02×10^{20}	1.25×10^{19}	1.85×10^{-14}	7.28×10^{-14}		9.13×10^{-14}	This work
1100	1800	9.40×10^{19}	9.68×10^{19}	1.65×10^{19}	8.16×10^{-14}	1.85×10^{-13}		2.67×10^{-13}	This work
1100	1800	1.10×10^{20}	1.12×10^{20}	1.65×10^{19}	6.30×10^{-14}	1.34×10^{-13}		1.96×10^{-13}	This work
1100	3600	9.40×10^{19}	9.68×10^{19}	1.65×10^{19}	8.16×10^{-14}	1.73×10^{-13}		2.55×10^{-13}	This work
1100	1500	4.00×10^{20}	4.01×10^{20}	1.65×10^{19}	1.23×10^{-13}	1.68×10^{-13}	2.53×10^{-15}	2.94×10^{-13}	49 and 50
1100	3600	7.80×10^{19}	8.13×10^{19}	1.65×10^{19}	8.70×10^{-14}	1.19×10^{-13}		2.06×10^{-13}	49 and 50
1100	28800	8.00×10^{18}	2.09×10^{19}	1.65×10^{19}	6.05×10^{-14}	8.27×10^{-14}		1.44×10^{-13}	49 and 50

$$D^*_{AsV^-} = \left(1.32^{+63.0}_{-1.30}\right)10^4 \exp\left(-\frac{(5.14\pm0.41)\ \text{eV}}{k_BT}\right)\ \text{cm}^2/\text{s}, \tag{26}$$

$$D^*_{P^0_i} = \left(2.53^{+23.4}_{-2.29}\right)\exp\left(-\frac{(3.68\pm0.25)\ \text{eV}}{k_BT}\right)\ \text{cm}^2/\text{s}, \tag{27}$$

$$D^*_{P^+_i} = \left(0.57^{+1.80}_{-0.43}\right)\exp\left(-\frac{(3.43\pm0.16)\ \text{eV}}{k_BT}\right)\ \text{cm}^2/\text{s}, \tag{28}$$

$$D^*_{PV^-} = \left(41.4^{+10303}_{-41.2}\right)\exp\left(-\frac{(4.44\pm0.59)\ \text{eV}}{k_BT}\right)\ \text{cm}^2/\text{s}. \tag{29}$$

These equations are illustrated in Figs. 9 and 10 by the solid lines. Both the results from modeling As diffusion in the Si isotope samples and As diffusion in natural Si were taken into account for the calculation of Eqs. (25) and (26). The contribution of AsI^0 pairs to As diffusion was set equal to the contribution of AsV^0 because As diffusion under intrinsic conditions is known to be almost equally enhanced both under V and I injection. The expressions of $D^*_{P^0_i}$ and $D^*_{P^+_i}$ given by Eqs. (27) and (28) include data obtained from modeling the simultaneous P and Si diffusion and P profiles in natural Si. The contribution of PV^- to P diffusion [see Eq. (29)] was deduced from fitting the high concentration P profiles given in the literature. In the case when only the results of $D^*_{P^0_i}$ and $D^*_{P^+_i}$ from the simultaneous diffusion of P and Si are taken into account we get

$$D^*_{P^0_i} = \left(6.79^{+37.7}_{-5.75}\right)10^2 \exp\left(-\frac{(4.36\pm0.21)\ \text{eV}}{k_BT}\right)\ \text{cm}^2/\text{s}, \tag{30}$$

$$D^*_{P^+_i} = \left(9.06^{+18.1}_{-6.04}\right)\exp\left(-\frac{(3.19\pm0.12)\ \text{eV}}{k_BT}\right)\ \text{cm}^2/\text{s}. \tag{31}$$

These equations are illustrated by the dashed lines in Fig. 10. Whereas Eqs. (28) and (31) are in good agreement within the experimental accuracy, Eqs. (27) and (30) reveal different activation enthalpies for P diffusion via P^0_i. This reflects the

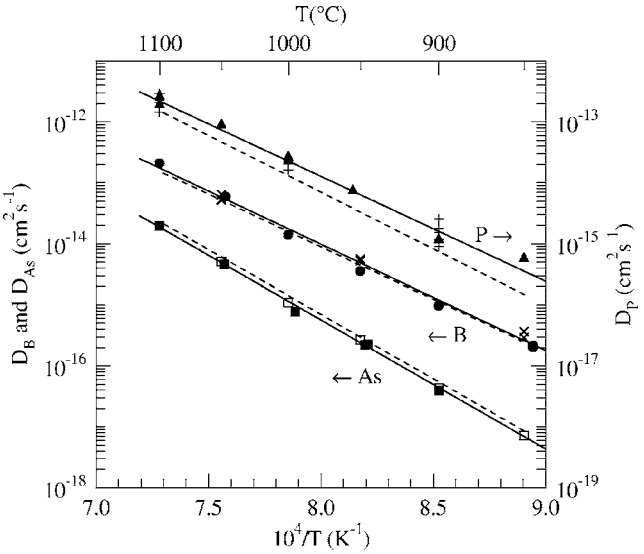

FIG. 8. Temperature dependence of the intrinsic diffusion coefficients of B (●, ×), As (■, □), and P (▲, +) in silicon. The solid lines are best fits of the respective intrinsic dopant-diffusion coefficients taking into account the results from modeling the simultaneous self- and dopant diffusion (●, ■, ▲) and from modeling the dopant profiles given in the literature (×, □, +). The dashed lines represent intrinsic diffusivities reported in the literature (B: Ref. 45; As: Ref. 26; P: Ref. 29). Note, the B and As diffusion data are referred to the left and the P diffusion data to the right axis of ordinate.

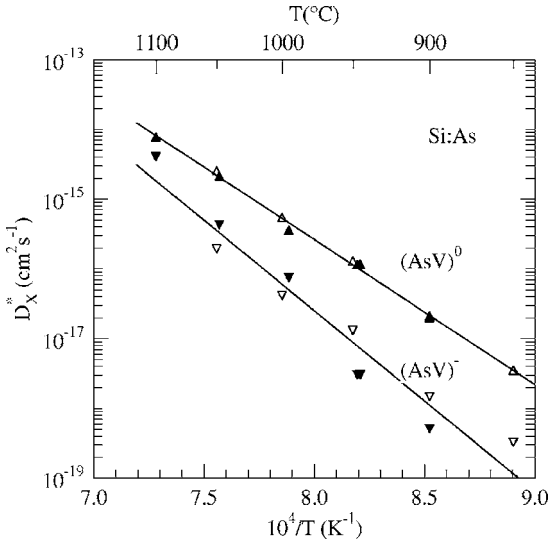

FIG. 9. Temperature dependence of the relative contributions D_X^* with $X=AsV^0$ (▲, △) and $X=AsV^-$ (▼, ▽) to As diffusion in Si under intrinsic conditions. Data illustrated by the full symbols were deduced from modeling the simultaneous diffusion of As and Si in Si isotope structures. Data given by the open symbols were obtained from fitting the As profiles given by Murota *et al.* (Refs. 47 and 48). The temperature dependence (solid lines) of the relative contributions are best reproduced by Eqs. (25) and (26). Note, $D^*_{AsI^0}=D^*_{AsV^0}$ was assumed for all simulations of As diffusion.

scatter in the data of $D^*_{P_i^0}$. The difference between $D^*_{P_i^0}$ deduced from the conventional and simultaneous diffusion experiments increases with decreasing temperature. Presumably, the in-diffusion of P from the top amorphous P-implanted Si layer into the crystalline isotope structure is retarded compared to P diffusion in natural Si, which was performed by means of variously doped oxide sources. This retardation could be associated with an active P concentration at the amorphous (crystalline) interface, which still increases during the diffusion process. With increasing active P concentration the impact of $D^*_{P_i^0}$ on P diffusion increases. Hence the P diffusion in the isotope structure could be slightly affected by a barrier at the top amorphous (crystalline) interface.

The energy levels determined for V and I are displayed in Fig. 11. Fitting of the experimental profiles reveals two donor levels for self-interstitials and two acceptor levels for vacancies. The positions of the two V acceptor levels are very close to each other. The experimental B and Si profiles are better described with a reverse-level ordering (negative-U) for the donor levels of the self-interstitials than with the regular-level ordering. This shows that I^{2+} dominates self-diffusion under p-type doping conditions and also mediates B diffusion. The experiments are not sensitive to the V donor levels, because B diffusion establishes a supersaturation of I and thereby suppresses the contribution of V to self-diffusion. However, an upper bound of 0.2 eV above the valence band could be deduced for the V levels. This is in agreement with the V donor levels $E^{+/++}=0.13$ eV and $E^{0/+}=0.05$ eV measured by Watkins.[51,52]

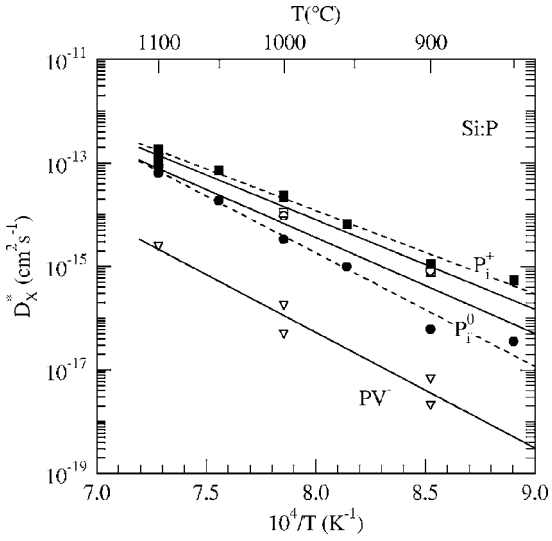

FIG. 10. Temperature dependence of the relative contributions D_X^* with $X=P_i^+$ (■, □), $X=P_i^0$ (●, ○), and $X=PV^-$ (▽) to P diffusion in Si under intrinsic conditions. The full and open symbols are the results from modeling the simultaneous diffusion of P and Si in Si isotope structures and from modeling P diffusion profiles given by Yoshida *et al.* (Refs. 49 and 50) respectively. The solid lines are the temperature dependence of the relative contributions, which are reproduced by Eqs. (27)–(29). The dashed lines given by Eqs. (30) and (31) show the temperature dependence of $D_{P_i^0}$ and $D_{P_i^+}$ in the case when only the data from the simultaneous diffusion study are taken into account.

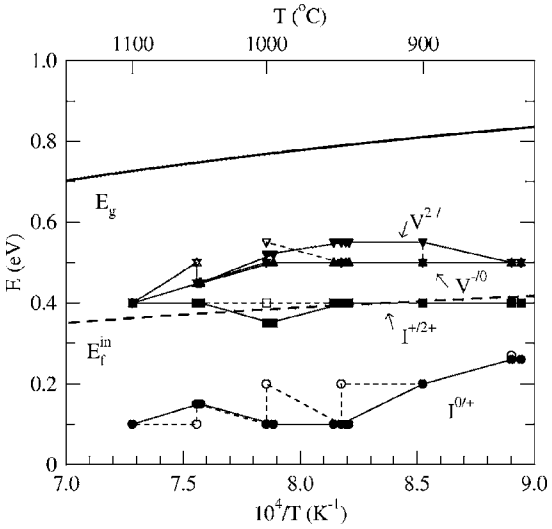

FIG. 11. Energy-level positions of vacancies V and self-interstitials I within the band gap of Si for temperatures between 850 and 1100 °C. The expressions given by Thurmond (Ref. 35) were used for the temperature dependence of the Si band gap [$E_g(T)$: upper thick solid line] and the Fermi level under intrinsic conditions [$E_f^{\mathrm{in}}(T)$: thick-dashed line]. The full and open symbols show the results from modeling the simultaneous self- and dopant diffusion shown in Figs. 2–4 and from modeling the dopant-diffusion profiles given in the literature (see Figs. 5–7), respectively. The thin solid and thin dashed lines are guides for the eye.

The transport coefficients $C_{V^k}^{\mathrm{eq}} D_{V^k}/C_o$ and $C_{I^u}^{\mathrm{eq}} D_{I^u}/C_o$, which result from the energy levels (see Sec. III A in Part I) and the above-mentioned constraints considered for the simulations [see Eqs. (14), (15), and (18)] are given in Table IV. The values deduced from the simulation of the B and P profiles given in the literature are also listed in Table IV (see data in brackets). They are in close agreement with the results of the simultaneous diffusion experiments. The transport capacities are displayed in Figs. 12 and 13. The data determined from modeling the simultaneous self- and dopant diffusion are best reproduced by the following expressions:

$$\frac{C_{I^0}^{\mathrm{eq}} D_{I^0}}{C_o} = \left(2732 \begin{matrix} +1235 \\ -850 \end{matrix}\right) \exp\left(-\frac{(4.96 \pm 0.04)\ \mathrm{eV}}{k_B T}\right)\ \mathrm{cm}^2/\mathrm{s}, \tag{32}$$

$$\frac{C_{I^+}^{\mathrm{eq}} D_{I^+}}{C_o} = \left(69.6 \begin{matrix} +310.7 \\ -56.9 \end{matrix}\right) \exp\left(-\frac{(4.82 \pm 0.18)\ \mathrm{eV}}{k_B T}\right)\ \mathrm{cm}^2/\mathrm{s}, \tag{33}$$

$$\frac{C_{I^{2+}}^{\mathrm{eq}} D_{I^{2+}}}{C_o} = \left(469 \begin{matrix} +3184 \\ -409 \end{matrix}\right) \exp\left(-\frac{(5.02 \pm 0.22)\ \mathrm{eV}}{k_B T}\right)\ \mathrm{cm}^2/\mathrm{s}, \tag{34}$$

TABLE IV. Data of the transport coefficients $C_{V^k}^{\mathrm{eq}} D_{V^k}/C_o$ and $C_{I^u}^{\mathrm{eq}} D_{I^u}/C_o$ of vacancies (V) and self-interstitials (I) which were determined from modeling the simultaneous self- and dopant diffusion in silicon isotope structures. The data refer to diffusion correlation factors of $f_{V^k}=0.5$ and $f_{I^u}=0.56$. The data in brackets are the values used to reproduce the B and P diffusion profiles shown in Fig. 5 and 7.

T (°C)	$C_{I^0}^{\mathrm{eq}} D_{I^0}/C_o$ ($\mathrm{cm}^2\ \mathrm{s}^{-1}$)	$C_{I^+}^{\mathrm{eq}} D_{I^+}/C_o$ ($\mathrm{cm}^2\ \mathrm{s}^{-1}$)	$C_{I^{2+}}^{\mathrm{eq}} D_{I^{2+}}/C_o$ ($\mathrm{cm}^2\ \mathrm{s}^{-1}$)	$C_{V^0}^{\mathrm{eq}} D_{V^0}/C_o$ ($\mathrm{cm}^2\ \mathrm{s}^{-1}$)	$C_{V^-}^{\mathrm{eq}} D_{V^-}/C_o$ ($\mathrm{cm}^2\ \mathrm{s}^{-1}$)	$C_{V^{2-}}^{\mathrm{eq}} D_{V^{2-}}/C_o$ ($\mathrm{cm}^2\ \mathrm{s}^{-1}$)	$C_{V^+}^{\mathrm{eq}} D_{V^+}/C_o$ ($\mathrm{cm}^2\ \mathrm{s}^{-1}$)	References
845	1.08×10^{-19}	2.03×10^{-20}	1.71×10^{-20}	1.39×10^{-19}	5.83×10^{-20}	2.45×10^{-20}	8.73×10^{-21}	This work
850	1.35×10^{-19}	2.58×10^{-20}	2.20×10^{-20}	1.72×10^{-19}	7.18×10^{-20}	3.00×10^{-20}	1.11×10^{-20}	This work
850	(1.30×10^{-19})	(2.89×10^{-20})	(2.46×10^{-20})	(1.72×10^{-19})	(7.18×10^{-20})	(3.00×10^{-20})	(1.11×10^{-20})	46
900	1.29×10^{-18}	1.69×10^{-19}	1.61×10^{-19}	1.39×10^{-18}	5.43×10^{-19}	1.30×10^{-19}	1.11×10^{-19}	This work
900	(1.29×10^{-18})	(1.69×10^{-19})	(1.61×10^{-19})	(1.39×10^{-18})	(5.43×10^{-19})	(1.30×10^{-19})	(1.11×10^{-19})	49 and 50
945	8.81×10^{-18}	5.26×10^{-19}	5.48×10^{-19}	7.49×10^{-18}	2.78×10^{-18}	6.38×10^{-19}	7.21×10^{-19}	This work
947	9.50×10^{-18}	5.73×10^{-19}	5.99×10^{-19}	8.05×10^{-18}	2.97×10^{-18}	6.83×10^{-19}	7.81×10^{-19}	This work
950	1.06×10^{-17}	6.50×10^{-19}	6.84×10^{-19}	8.96×10^{-18}	3.30×10^{-18}	7.56×10^{-19}	8.80×10^{-19}	This work
950	(9.05×10^{-18})	(1.43×10^{-18})	(1.50×10^{-18})	(8.68×10^{-18})	(3.19×10^{-18})	(1.18×10^{-18})	(8.51×10^{-19})	46
955	1.29×10^{-17}	8.02×10^{-19}	8.52×10^{-19}	1.07×10^{-17}	3.92×10^{-18}	8.94×10^{-19}	1.07×10^{-18}	This work
995	5.63×10^{-17}	4.14×10^{-18}	3.00×10^{-18}	4.12×10^{-17}	1.44×10^{-17}	4.20×10^{-18}	4.79×10^{-18}	This work
1000	6.71×10^{-17}	5.03×10^{-18}	3.68×10^{-18}	4.85×10^{-17}	1.69×10^{-17}	4.90×10^{-18}	5.74×10^{-18}	This work
1000	(5.41×10^{-17})	(1.01×10^{-17})	(1.16×10^{-17})	(4.93×10^{-17})	(1.72×10^{-17})	(3.79×10^{-18})	(5.83×10^{-18})	49 and 50
1047	2.87×10^{-16}	4.00×10^{-17}	5.02×10^{-17}	1.73×10^{-16}	8.88×10^{-17}	4.56×10^{-17}	2.41×10^{-17}	This work
1048	2.97×10^{-16}	4.15×10^{-17}	5.21×10^{-17}	1.78×10^{-16}	9.14×10^{-17}	4.69×10^{-17}	2.49×10^{-17}	This work
1050	3.16×10^{-16}	4.45×10^{-17}	5.16×10^{-17}	1.89×10^{-16}	9.69×10^{-17}	4.96×10^{-17}	2.66×10^{-17}	This work
1050	(3.16×10^{-16})	(4.45×10^{-17})	(5.16×10^{-17})	(1.89×10^{-16})	(9.69×10^{-17})	(4.96×10^{-17})	(2.66×10^{-17})	46
1100	1.61×10^{-15}	1.75×10^{-16}	2.39×10^{-16}	6.26×10^{-16}	4.58×10^{-16}	3.35×10^{-16}	1.03×10^{-16}	This work
1100	(1.61×10^{-15})	(1.75×10^{-16})	(2.39×10^{-16})	(6.26×10^{-16})	(4.58×10^{-16})	(3.35×10^{-16})	(1.03×10^{-16})	49 and 50

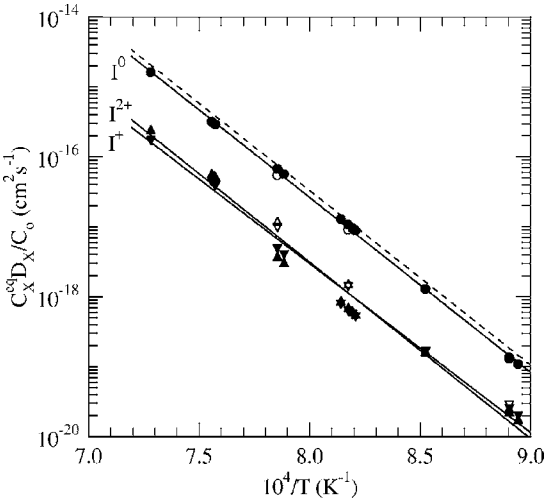

FIG. 12. Temperature dependence of the transport coefficients $C_{I^u}^{eq}D_{I^u}/C_o$ of I^0 (●), I^+ (▼) and I^{2+} (▲), which were deduced from modeling the simultaneous diffusion of self- and dopant atoms in Si isotope multilayer structures. The open symbols are the data from modeling the B and P profiles shown in Figs. 5 and 7. The solid lines are reproduced by Eqs. (32)–(34). The dashed line is the sum of all contributions, which is given by Eq. (15).

$$\frac{C_{V^0}^{eq}D_{V^0}}{C_o} = \left(13.3^{+9.8}_{-5.6}\right)\exp\left(-\frac{(4.42\pm0.06)\ \text{eV}}{k_BT}\right)\ \text{cm}^2/\text{s}, \tag{35}$$

$$\frac{C_{V^-}^{eq}D_{V^-}}{C_o} = \left(38.9^{+15.1}_{-10.9}\right)\exp\left(-\frac{(4.63\pm0.04)\ \text{eV}}{k_BT}\right)\ \text{cm}^2/\text{s}, \tag{36}$$

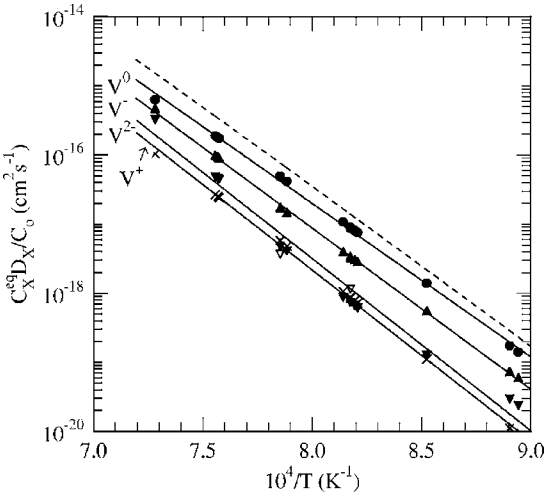

FIG. 13. Temperature dependence of the transport coefficients $C_{V^u}^{eq}D_{V^u}/C_o$ of V^0 (●), V^- (▲), V^{2-} (▼), and V^+ (×) which were deduced from modeling the simultaneous diffusion of self- and dopant atoms in Si isotope multilayer structures. The open symbols are the results from modeling the B and P profiles shown in Figs. 5 and 7. The solid lines are reproduced by Eqs. (35)–(38). The dashed line is the sum of all contributions, which is given by Eq. (18).

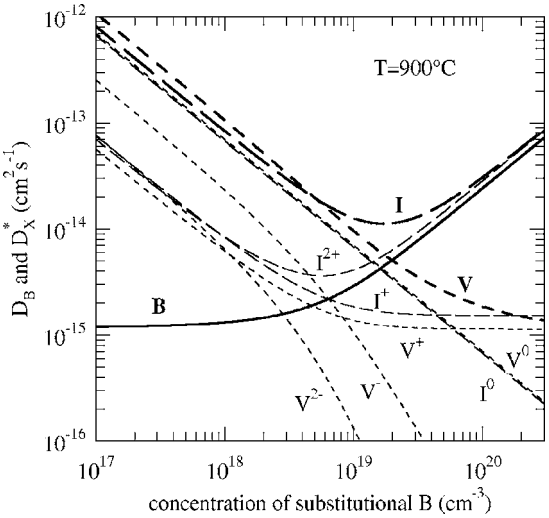

FIG. 14. The B diffusion coefficient $D_B(=D_{B_i^0}^*)$ and the reduced-diffusion coefficient D_X^* of the point defect X with $X \in \{V^+, V^0, V^-, V^{2-}, I^{2+}, I^+, I^0\}$ as a function of the B concentration $C_{B_s^-}^{eq}$ for 900 °C. The acceptor concentration dependence of D_B is shown by the thick solid line. The total reduced-diffusion coefficients D_V^* and D_I^* are illustrated by the thick short-dashed and thick wide-dashed lines, respectively. The relative contributions to D_V^* (D_I^*) are given by the thin short-dashed lines (thin wide-dashed lines).

$$\frac{C_{V^{2-}}^{eq}D_{V^{2-}}}{C_o} = \left(240^{+1473}_{-207}\right)\exp\left(-\frac{(4.93\pm0.21)\ \text{eV}}{k_BT}\right)\ \text{cm}^2/\text{s}, \tag{37}$$

$$\frac{C_{V^+}^{eq}D_{V^+}}{C_o} = \left(150^{+109}_{-63}\right)\exp\left(-\frac{(4.92\pm0.06)\ \text{eV}}{k_BT}\right)\ \text{cm}^2/\text{s}. \tag{38}$$

The sum of Eqs. (32)–(34) agrees closely with the value of Eq. (15) and the sum of Eqs. (35)–(37) with that of Eq. (18). The values used to describe the dopant profiles given in the literature were not taken into account because these profiles are less sensitive to native-defect properties than the profiles from the simultaneous diffusion study. The contribution of I^- to self-diffusion under intrinsic conditions is more than three orders of magnitude lower than the contributions of the positively charged self-interstitials. Hence the I^- contribution is not relevant for self-diffusion via self-interstitials and is omitted.

VI. DISCUSSION

The dopant and self-atom profiles analyzed in this work provide comprehensive information about the properties of the point defects involved in the dopant-diffusion process. Taking into account our results the diffusion behavior of B, As, and P can be predicted for various experimental conditions. Figures 14–16 illustrate the doping dependence of the diffusion of B, As, P, respectively, and of the native-point

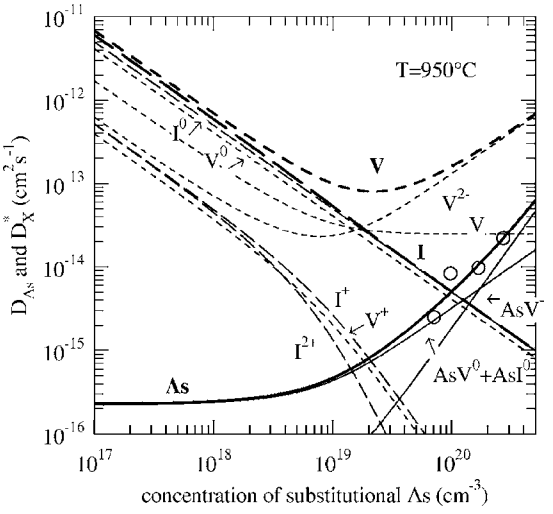

FIG. 15. The total As diffusion coefficient $D_{\mathrm{As}}(=D^*_{\mathrm{As}V^0}+D^*_{\mathrm{As}I^0}+D^*_{\mathrm{As}V^-})$ and the reduced-diffusion coefficient D^*_X $(X \in \{\mathrm{As}V^0, \mathrm{As}V^-, \mathrm{As}I^0, V^+, V^0, V^-, V^{2-}, I^{2+}, I^+, I^0\})$ as a function of the As concentration $C^{\mathrm{eq}}_{\mathrm{As}^+_s}$ for 950 °C. The thick solid line shows the concentration dependence of D_{As}. The total reduced-diffusion coefficients D^*_V and D^*_I are illustrated by the thick short-dashed and thick wide-dashed lines, respectively. The relative contributions to D^*_V (D^*_I) are given by the thin short-dashed lines (thin wide-dashed lines). The symbol (○) shows data of D_{As} from isoconcentration diffusion experiments (Ref. 26).

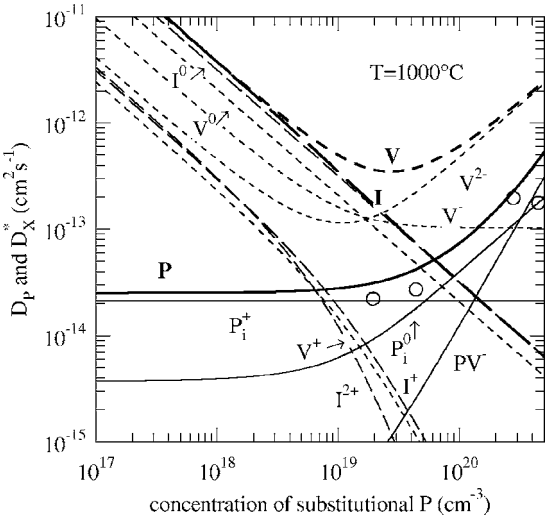

FIG. 16. The total P diffusion coefficient $D_{\mathrm{P}}(=D^*_{\mathrm{P}^+_i}+D^*_{\mathrm{P}^0_i}+D^*_{\mathrm{P}V^-})$ and the reduced-diffusion coefficient D^*_X $(X \in \{\mathrm{P}^+_i, \mathrm{P}^+_i, \mathrm{P}V^-, V^+, V^0, V^-, V^{2-}, I^{2+}, I^+, I^0\})$ as a function of the P concentration $C^{\mathrm{eq}}_{\mathrm{P}^+_s}$ for 1000 °C. The thick solid line is the concentration dependence of D_{P}. D^*_V and D^*_I are illustrated by the thick short-dashed and thick wide-dashed lines, respectively. The relative contributions to D^*_V (D^*_I) are given by the thin short-dashed lines (thin wide-dashed lines). The symbol (○) shows data of D_{P} from isoconcentration diffusion experiments (Ref. 29).

defects. $D_{\mathrm{B}}=D^*_{\mathrm{B}^0_i}$ (thick solid line) increases linearly with increasing B concentration above the intrinsic carrier concentration (see Fig. 14). The total reduced-diffusion coefficients $D^*_I=C^{\mathrm{eq}}_I D_I/C^{\mathrm{eq}}_{\mathrm{B}^-_s}$ and $D^*_V=C^{\mathrm{eq}}_V D_V/C^{\mathrm{eq}}_{\mathrm{B}^-_s}$ as a function of the B concentration are shown by the thick long-dashed and thick short-dashed lines, respectively. The reduced diffusivities of $I^u(V^k)$ are given by the thin long-dashed lines (thin short-dashed lines). Figure 14 demonstrates that under high B doping levels, B diffusion and self-diffusion are mainly mediated by I^{2+}. At low acceptor concentrations D_{B} is several orders of magnitude smaller than D^*_I and D^*_V. Accordingly, B diffusion proceeds in the foreign-atom-controlled mode. With increasing acceptor concentrations D_{B} exceeds D^*_V and approaches D^*_I. At high acceptor concentrations a native-defect-controlled diffusion mode is established, that is, B diffusion leads to native-defect concentrations deviating from thermal equilibrium.

Figure 15 shows the doping dependence of the diffusion of point defects involved in As diffusion. The thick solid line represents the total As diffusivity D_{As}. The doping dependence of D_{As} accurately describes previous results, which were obtained by isoconcentration diffusion experiments[26] (see open symbols in Fig. 15). The contributions of $\mathrm{As}V^0$, $\mathrm{As}I^0$ and $\mathrm{As}V^-$ to D_{As} [see Eq. (20)] are given by the thin solid lines. The total reduced-diffusion coefficients D^*_I and D^*_V are displayed by the thick long- and short-dashed lines, respectively. The thin long- and short-dashed lines are the corresponding relative contributions to the total diffusivities. For high As concentrations negatively charged vacancies mainly mediate As and self-diffusion. The magnitude of $D^*_{V^-}$ and $D^*_{V^{2-}}$ exceeds D_{As} for all doping levels. The foreign-atom-controlled mode of As diffusion holds for all As concentrations, that is, As diffusion proceeds under thermal equilibrium of I and V.

The total diffusion coefficient of P and the contributions to D_{P} are displayed in Fig. 16. The doping dependence calculated for D_{P} fairly well reproduces data from isoconcentration studies reported by Makris and Masters.[29] Compared to these former results we obtained always slightly higher values for D_{P} which, however, are within a factor of 2 consistent with the previous results. The reason for the difference is unclear. It may just reflect the limited accuracy of both studies or a systematic underestimation of previous results. Figure 4 demonstrates that the P diffusivity for high donor concentrations is mainly determined by $\mathrm{P}V^-$ and P^0_i whereas under intrinsic conditions the contribution due to P^+_i dominates. Concerning the diffusion mode established by P diffusion, a foreign-atom-controlled mode holds for low donor concentrations. For P concentrations exceeding 10^{19} cm^{-3} P diffusion becomes native-defect controlled. Although D_{P} and D_{B} are very similar in magnitude at the same temperature and doping level (see Figs. 2 and 4), the supersaturation of I established by P diffusion is lower than in the case of B diffusion. This is explained with the increasing impact of vacancies on P diffusion with increasing donor concentration.

Taking into account the relative contributions to Si self-diffusion, which for intrinsic conditions are given by Eqs. (32)–(38), their doping dependence can be calculated by means of Eq. (71) given in Part I. Figure 17 shows the relative contributions (dashed lines) to the total Si self-diffusion

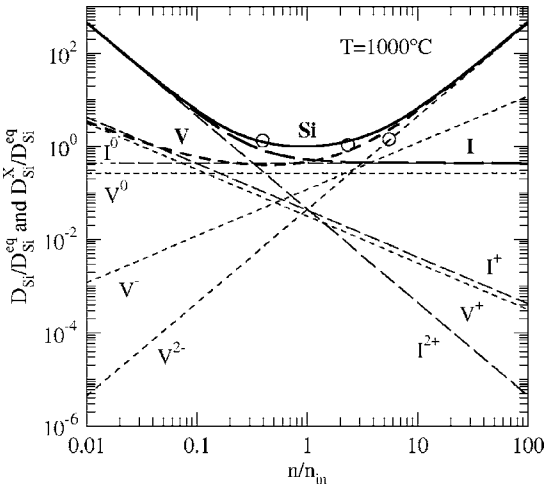

FIG. 17. Doping dependence of the relative contributions (dashed lines) to the total Si self-diffusion coefficient (solid line) at 1000 °C. Both the relative contributions and the total Si self-diffusion coefficient were normalized to the intrinsic equilibrium self-diffusion coefficient D_{Si}^{eq}, which is given by Eq. (14). The relative contributions of charged vacancies and self-interstitials are given by the thin short-dashed and thin wide-dashed lines, respectively. The thick short-dashed line (thick wide-dashed line) represents the sum of all vacancy (self-interstitial) contributions to self-diffusion. The doping dependence of the total self-diffusion coefficient (thick solid line) determined in this work reproduces experimental results (○) reported by Ural *et al.* (Ref. 53).

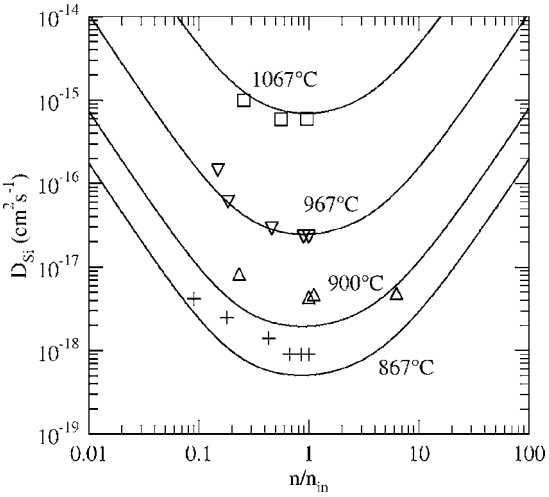

FIG. 18. Doping dependence of the Si self-diffusion coefficient D_{Si} (solid lines) for various temperatures. Data on extrinsic Si diffusion given in the literature [symbols (Refs. 54–56)] are in fairly good agreement with our results.

coefficient (solid line) at 1000 C°. The correlation factors $f_{I^u}=0.56$ and $f_{V^k}=0.5$ were considered for the calculation of the total self-diffusion coefficient. The doping dependence of D_{Si} shown in Fig. 17 reproduces the experimental results of Ural *et al.*[53] fairly well. In addition, the results reported by Nakabayashi *et al.*[54,55] and Matsumoto *et al.*.[56] on Si self-diffusion under extrinsic conditions are also described as demonstrated by Fig. 18. The data for 867 and 900 °C shown in Fig. 18 suggest a factor of two higher self-diffusion even under intrinsic conditions. These data are very likely too high because the intrinsic Si diffusion was accurately determined recently by means of well-designed isotope structures.[10] The doping dependence of the relative contributions to self-diffusion (see Fig. 17) reveals that self-interstitials and vacancies mainly determine Si self-diffusion under high *p*-type ($n/n_{in}<1$) and high *n*-type doping ($n/n_{in}>1$), respectively.

The energy-level scheme derived in this work for high temperatures is very similar to the level ordering predicted by theory for zero K. Total energy calculations of the formation enthalpy of vacancies and self-interstitials predict donor and acceptor states for both types of defects.[37,57] Our experiments confirm the existence of *V* acceptor states in the upper half of the Si band gap and *V* donor states in the lower half. Moreover, a reversed level ordering for the donor levels introduced by self-interstitials is suggested that was already predicted theoretically by Car *et al.*[57] Altogether the type and charge states of the native-point defects deduced from modeling dopant diffusion in Si isotope multilayers are in agreement with theoretical predictions. In addition, our study yields information about the temperature dependence of the defect levels (see Fig. 11). These results may stimulate further calculations of the temperature shift of defect states.

In accord with *ab initio* calculations of Zhu *et al.*[21] we assumed the kick-out mechanism for B diffusion in Si. However, more recent first-principle calculations based on density-functional theory indicate that B diffusion is mediated by the interstitialcy mechanism,[22–25] that is, the mobile defect is a B*I* pair rather than a B interstitial (B_i). An activation enthalpy of 3.45 eV (3.61 eV) for B diffusion via neutral BI^0 pairs was calculated by Windl *et al.*[23] within the local-density approximation (generalized-gradient approximation), which is in excellent agreement with our experimental result of 3.46 eV given by Eq. (22). Although this agreement provides additional evidence for the interstitialcy mechanisms, it is still not yet a proof because the activation enthalpy for B diffusion mediated by the kick-out mechanism is very similar.[23] Assuming that B diffuses via mobile B*I* pairs rather than via B_i, our experiments should indicate a contribution of B*I* pairs to self-diffusion because the transport capacity $C_{BI^0}^{eq}D_{BI^0}$ exceeds that of *V* and *I* [see Eq. (74) in Part I]. However, the analysis of the simultaneous diffusion of B and Si did not reveal any significant contribution of B*I* pairs to self-diffusion. This indicates that the correlation factor f_{BI^0} of self-diffusion via B*I* pairs must be small (below 0.5). Note, no correlation, i.e., $f_{BI^0}=0$, also implies that B diffuses via the kick-out mechanism because the lifetime of B*I* pairs is then zero. In order to positively confirm the kick-out mechanism for B diffusion in Si, calculations of the correlation factor of self-diffusion via B*I* pairs are necessary. In the case when these calculations yield a correlation factor close to one, B diffusion in Si is mediated by the kick-out mechanism, because the simultaneous diffusion experiments did not reveal a contribution of B*I* pairs to self-diffusion.

An activation enthalpy of 3.42 eV is obtained for the total intrinsic diffusion of P in Si [see Eq. (24)]. This intrinsic diffusivity is made up of contributions due to P_i^0, P_i^+, and PV^-

[see Eqs. (21) and (27)–(29)]. The activation enthalpies of the relative contributions are 3.68 eV (P_i^0), 3.43 eV (P_i^+), and 4.44 eV (PV^-). Recent first-principles density-functional-theory calculations of Liu *et al.*[58] not only support the existence of P_i^0 and P_i^+ but also provide activation enthalpies of P diffusion via these defects. The authors determined 3.5 eV for intrinsic P diffusion via P_i^0 and 3.4 eV for P diffusion via P_i^+. This excellent agreement with our results supports the P interstitial mediated diffusion of P under intrinsic conditions. For the PV^- contribution to P diffusion Liu *et al.*[58] calculated an activation enthalpy of 3.4 eV, which is at variance with our value of 4.44 eV. Liu *et al.* pointed out that their result for PV^- only represent a lower bound because the calculation performed within the local-density approximation (LDA) and generalized-gradient approximation (GGA) both predict Si band gaps which are too small. As a consequence, the formation enthalpy of PV^- (2.2 eV)[58] (which, beside the migration enthalpy of the pair, determines the activation enthalpy), is likely underestimated.

In the case of As, Eqs. (25) and (26) suggest activation enthalpies of 4.12 and 5.14 eV for As diffusion via AsV^0 and AsV^- pairs. Taking into account the formation enthalpy of 2.37 eV and migration enthalpy of 1.19 eV for AsV^0 pairs calculated by Xie and Chen,[59,60] an activation enthalpy of 3.56 eV is obtained for As diffusion. Presumably, as in the case of P*V* pairs, the calculated value is too low. Corresponding theoretical results for As diffusion via AsV^- are not reported in the literature to the authors knowledge.

Currently accurate predictions of activation energies of dopant diffusion via dopant-vacancy pairs seem to be lacking. This includes calculations of the activation enthalpy of self-diffusion via vacancies. According to Sec. IV E the activation enthalpy of Si self-diffusion via vacancies is estimated to be 4.3 or 4.6 eV, depending on the correlation factor assumed for self-diffusion via self-interstitials. The activation enthalpy equals the sum of the *V* formation and migration enthalpies. Most recent *ab initio* calculations yield 3.3 (Ref. 61) and 3.17 eV (Ref. 62) for the formation enthalpy of the neutral *V*. On the other hand, theory predicts an energy barrier of 0.4 eV for vacancy hops to the nearest neighbors,[64] which is in agreement with the experimental results of Watkins.[51,52] Taking into account these most recent theoretical results we obtain 3.17 eV+0.4 eV=3.57 eV for the activation enthalpy of Si self-diffusion via vacancies, which is clearly at variance with experimental results, which suggest values above 4 eV. This disagreement between theory and experiment on *V*-mediated self-diffusion is also apparent in the activation enthalpy of dopant diffusion. For example, Sb mainly diffuses by a *V*-mediated mechanism with an activation enthalpy of 4.08 eV.[65] According to Dunham and Wu[66] the difference between the activation enthalpy of self-diffusion by vacancies and the diffusion-activation enthalpy of the dopant-vacancy pair is associated with the binding energies between the substitutional dopant and the *V* in the second and third nearest-neighbor positions. Assuming either 4.3 or 4.6 eV for self-diffusion by vacancies a difference of 0.22 or 0.52 eV is obtained. In the case when the theoretical estimate of 3.57 eV for self-diffusion via vacancies is assumed (see above) a negative binding energy between Sb and *V* is obtained, which is in conflict with the established *V*-mediated diffusion of Sb. The diffusion of dopant-vacancy pairs also suggests an activation enthalpy for self-diffusion via vacancies above 4.0 eV. Obviously, the deficiency of first-principle density-functional-theory calculations within LDA and GGA to calculate the band-gap energy exhibit severe problems to accurately predict the formation enthalpy of vacancies and dopant-vacancy pairs. Whether band-gap corrections will provide a higher *V*-formation energy that is required to end up with an activation enthalpy of *V*-mediated self-diffusion above 4 eV remains to be seen in the future.

On the other hand, one may argue that the value of 3.3 (Ref. 61) and 3.17 eV (Ref. 62) predicted by theory for the formation of a neutral *V* is correct since this value is supported by recent positron-annihilation analyses of *V* formation in highly As- and P-doped silicon, which yielded (2.8±0.3) eV.[63] In this case the calculated migration energy of 0.4 eV (Ref. 64) does not represent the migration energy at high temperatures. In fact, recent radiation-enhanced self-diffusion (RESD) experiments show that vacancies at high temperatures diffuse with a migration enthalpy of (1.8±0.5) eV.[31] Taking into account this value and the theoretical estimate of the *V*-formation enthalpy, an activation enthalpy of Si diffusion via vacancies in the range between 4.5 and 5.5 eV is obtained, which is consistent with the activation enthalpy obtained in this work for self- and dopant diffusion via vacancies. However, the high migration enthalpy of vacancies at high temperatures is at variance with the low migration barrier found for vacancies at low temperatures.[51,52] Assuming the low- and high-temperature properties of vacancies are correct, the entropy and enthalpy of *V* migration must increase with increasing temperature. This interpretation would satisfy the concept of a spread out defect first proposed by Seeger and Chik already in 1968.[67] This seems to be a reasonable explanation but theoretical calculations cannot confirm *V* migration barriers above 1 eV.

Finally, a third approach is worth considering to unravel the apparent inconsistency between the theoretical and experimental estimate of the activation enthalpy of *V*-mediated self- and dopant diffusion. Assuming the theoretical results of the properties of vacancies in Si to be correct, the inconsistency between theory and experiment may indicate that the native defect mediating the diffusion at elevated temperatures is not an isolated *V* but rather a divacancy (V_2). This approach is supported by the migration enthalpy of (1.8±0.5) eV, which was recently determined by radiation-enhanced self-diffusion (RESD) experiments.[31] Within experimental accuracy the value is consistent with 1.3 eV, which was determined both experimentally[68–70] and theoretically[71] for the migration barrier of V_2 in Si. Taking into account recent calculations of Hwang *et al.*[71] of the diffusion and dissociation of neutral V_2 in Si, a migration enthalpy of 1.35 eV and formation enthalpy of 5.22 eV is obtained. These values suggest an activation enthalpy for self-diffusion via V_2 of 6.57 eV. Although this value is certainly too high compared to the activation enthalpy of self-diffusion via *V* determined in this work [see Eq. (18)], the divacancy concept can explain activation enthalpies of vacancy-mediated dopant diffusion above 4 eV and, as already mentioned, the migration enthalpy of the vacancy-

related defect mediating RESD. However, the V_2 concept bears major consequences for our understanding of vacancy-mediated dopant diffusion. In order to prove or disprove this approach, extensive simulations of self- and dopant diffusion must be performed on the basis of this approach. This will show whether dopant diffusion and, in particular, also the simultaneous self- and dopant diffusion can be accurately and consistently described. This, however, is beyond the scope of this paper and thus will be prepared for publication elsewhere.

VII. CONCLUSION

The simultaneous diffusion of dopants and self-atoms and the different diffusion modes established by the *n*- and *p*-type dopants lead to concentration profiles that are sensitive to the properties of native-point defects. The advantage of the comprehensive diffusion study described in this work compared to former analyses is that the simulation of dopant diffusion in the isotope structure comprises all dopants and the corresponding self-atom profiles. The charge states of vacancies and self-interstitials were deduced and the relative contributions of the native-point defects and mobile dopant defects to self- and dopant diffusion were determined. Accurate simulations were performed with a diffusion-correlation factor of 0.56 for self-diffusion via self-interstitials. This value, which is at variance with the commonly used value of 0.73,[38] is in agreement with recent molecular dynamic results.[39,40] The activation enthalpy of vacancy-mediated self-diffusion, which was determined to 4.56 eV, is more consistent with the activation enthalpy of vacancy-mediated dopant diffusion than earlier results. Making allowance for the fact that the band-gap and the energy levels change with temperature, an energy-level diagram of the native-point defects is obtained that is essentially equal to that predicted by theory. In agreement with our present understanding on dopant diffusion in Si, B diffusion is mainly mediated by self-interstitials whereas the properties of both vacancies and self-interstitials are important to model As and P diffusion. No significant contribution of BI^0 pairs to Si self-diffusion was found, suggesting either a small diffusion-correlation factor f_{BI^0} or that B diffuses via the kick-out mechanism rather than via the interstitialcy mechanism. The simultaneous diffusion of *P* and Si shows that the tail of extrinsic *P* profiles is not, as hitherto accepted, caused by a supersaturation of self-interstitials. In fact, the tail region is mainly affected by singly positively charged mobile *P* defects. It is the mobility of this defect and the supersaturation of self-interstitials that determine the tail of extrinsic *P* diffusion profiles. The dopant-diffusion coefficients reduced to electronically intrinsic conditions are in good agreement with data of the intrinsic diffusivity of the dopant reported in the literature. Altogether our results obtained from the analysis of the simultaneous self- and dopant diffusion and from the analysis of dopant profiles given in the literature provide overall consistent data for modeling dopant and self-diffusion in Si for various experimental conditions.

The comparison between experimental and theoretical results of the activation enthalpy of self- and dopant diffusion shows good agreement for diffusion via the kick-out and interstitialcy mechanisms but significant differences for vacancy-mediated self- and dopant diffusion. In general, theory predicts activation enthalpies too low for self- and dopant diffusion via vacancies. This inconsistency either reflects a deficiency of first-principle calculations to accurately predict the band-gap energy of semiconductors or points to a still-remaining lack in our understanding of diffusion in Si. In order to unravel the inconsistency more sophisticated theoretical calculations are required to solve the energy band-gap problem. On the other hand, assuming that the theory is correct, the disagreement could indicate that the impact of, for example, divacancies on self- and dopant diffusion is more significant than generally expected. Putting forward both theoretical calculations on the properties of point defects in Si and the concept of more complex native defects involved in diffusion, the disagreement between theoretical and experimental results on vacancy-mediated diffusion should be resolved.

ACKNOWLEDGMENTS

The authors acknowledge J. Lundsgaard Hansen (University of Aarhus, Denmark) for the growth of the amorphous Si layer on top of the Si isotope multilayer structure and A. Nylandsted Larsen (University of Aarhus, Denmark), M. Posselt (Research Center Rossendorf, Dresden) and W. Windl (Ohio State University, USA) for valuable discussions. This work was supported by the Deutsche Forschungsgemeinschaft and in part by industry and the State of California under the UC Discovery Grant, by US NSF Grant No. DMR-0405472, and by the Director, Office of Science, Office of Basic Energy Sciences, Division of Materials Sciences and Engineering, of the U.S. Department of Energy under Contract No. DE-AC02-05CH11231.

*Electronic address: bracht@uni-muenster.de

[1] H. Bracht and N. A. Stolwijk, *Solubility in Silicon and Germanium*, Landolt-Börnstein New Series, Vol. III/41, Subvolume A2α (Springer, New York, 2002).

[2] N. A. Stolwijk and H. Bracht, *Diffusion in Silicon, Germanium and their Alloys*, Landolt-Börnstein New Series, Vol. III/33, Subvolume A (Springer, New York, 1998).

[3] P. M. Fahey, P. B. Griffin, and J. D. Plummer, Rev. Mod. Phys. **61**, 289 (1989).

[4] M. Uematsu, J. Appl. Phys. **82**, 2228 (1997).

[5] H. H. Silvestri, doctoral thesis, UC Berkeley, 2004.

[6] I. D. Sharp, H. A. Bracht, H. H. Silvestri, S. P. Nicols, J. W. Beeman, J. Hansen, A. Nylandsted Larsen, and E. E. Haller, MRS Symposia Proceedings No. 719 (Materials Research Soci-

ety, Pittsburgh, PA, 2002), p. F13.11.
[7] H. H. Silvestri, I. D. Sharp, H. A. Bracht, S. P. Nicols, J. W. Beeman, J. Hansen, A. Nylandsted Larsen, and E. E. Haller, MRS Symposia Proceedings No. 719 (Materials Research Society, Pittsburgh, PA, 2002), p. F13.10.
[8] H. Bracht, H. H. Silvestri, I. D. Sharp, S. P. Nicols, J. W. Beeman, J. L. Hansen, A. Nylandsted Larsen, and E. E. Haller, Inst. Phys. Conf. Ser. **171**, C3.8 (2003).
[9] H. H. Silvestri, H. Bracht, I. D. Sharp, J. Lundsgaard Hansen, A. Nylandsted Larsen, and E. E. Haller, MRS Symposia Proceedings No. 810 (Materials Research Society, Pittsburgh, PA, 2004), p. C3.3.
[10] H. Bracht, E. E. Haller, and R. Clark-Phelps, Phys. Rev. Lett. **81**, 393 (1998).
[11] H. Bracht, E. E. Haller, K. Eberl, M. Cardona, and R. Clark-Phelps, MRS Symposia Proceedings No. 527 (Materials Research Society, Pittsburgh, PA, 1998), p. 335.
[12] H. Bracht, Physica B **376-377**, 11 (2006).
[13] M. Yoshida and S. Tanaka, Jpn. J. Appl. Phys., Part 1 41, 5493 (2002).
[14] S. Matsumoto, Y. Ishikawa, and T. Niimi, J. Appl. Phys. **54**, 5049 (1983).
[15] Y. Ishikawa, I. Nakamichi, S. Matsumoto, and T. Niimi, Jpn. J. Appl. Phys., Part 1 26, 1602 (1987).
[16] S. Mizuo, T. Kusaka, A. Shintani, M. Nanba, and H. Higuchi, J. Appl. Phys. **54**, 3860 (1983).
[17] P. Fahey, G. Barbuscia, M. Moslehi, and R. W. Dutton, Appl. Phys. Lett. **46**, 784 (1985).
[18] H.-J. Gossmann, T. E. Haynes, P. A. Stolk, D. C. Jacobson, G. H. Gilmer, J. M. Poate, H. S. Luftman, T. K. Mogi, and M. O. Thompson, Appl. Phys. Lett. **71**, 3862 (1997).
[19] M. Miyake, J. Appl. Phys. **57**, 1861 (1985).
[20] N. E. B. Cowern, G. F. A. van de Walle, D. J. Gravesteijn, and C. J. Vriezema, Phys. Rev. Lett. **67**, 212 (1991).
[21] J. Zhu, T. Diaz de la Rubia, L. H. Yang, C. Mailhiot, and G. H. Gilmer, Phys. Rev. B **54**, 4741 (1996).
[22] B. Sadigh, T. J. Lenosky, S. K. Theiss, M.-J. Caturla, T. Diaz de la Rubia, and M. A. Foad, Phys. Rev. Lett. **83**, 4341 (1999).
[23] W. Windl, M. M. Bunea, R. Stumpf, S. T. Dunham, and M. P. Masquelier, Phys. Rev. Lett. **83**, 4345 (1999).
[24] P. Alippi, L. Colombo, P. Ruggerone, A. Sieck, G. Seifert, and Th. Frauenheim, Phys. Rev. B **64**, 075207 (2001).
[25] Ji-Wook Jeong and Atsushi Oshiyama, Phys. Rev. B **64**, 235204 (2001).
[26] B. J. Masters and J. M. Fairfield, J. Appl. Phys. **40**, 2390 (1969).
[27] T. Y. Tan and U. Gösele, Ann. Phys. (N.Y.) **A37**, 1 (1985).
[28] R. B. Fair and J. C. C. Tsai, J. Electrochem. Soc. **124**, 1107 (1977).
[29] J. S. Makris and B. J. Masters, J. Electrochem. Soc. **120**, 1252 (1973).
[30] H. Bracht, N. A. Stolwijk, and H. Mehrer, Phys. Rev. B **52**, 16542 (1995).
[31] H. Bracht, J. F. Pedersen, N. Zangenberg, A. N. Larsen, E. E. Haller, G. Lulli, and M. Posselt, Phys. Rev. Lett. **91**, 245502 (2003).
[32] L. Lerner and N. A. Stolwijk, Appl. Phys. Lett. **86**, 011901 (2005).
[33] S. Obeidi and N. A. Stolwijk, Phys. Rev. B **64**, 113201 (2001).
[34] R. Falster, V. V. Voronkov, and F. Quast, Phys. Status Solidi B **222**, 219 (2000).
[35] C. D. Thurmond, J. Electrochem. Soc. **122**, 1133 (1975).
[36] K. Compaan and Y. Haven, Trans. Faraday Soc. **52**, 786 (1956).
[37] G. M. Lopez and V. Fiorentini, Phys. Rev. B **69**, 155206 (2004).
[38] K. Compaan and Y. Haven, Trans. Faraday Soc. **54**, 1498 (1958).
[39] M. Posselt, F. Gao, and D. Zwicker, Phys. Rev. B **71**, 245202 (2005).
[40] Results of Posselt *et al.* (Ref. 39) for the diffusivity of the monointerstitial and the self-diffusion via these defects provide 0.54 for the diffusion-correlation factor (see, Table II in Ref. 39). Additional calculations of Posselt (unpublished) yield 0.56 rather than 0.54 for f_I.
[41] S. J. Clark and G. J. Ackland, Phys. Rev. B **56**, 47 (1997).
[42] O. K. Al-Mushadani and R. J. Needs, Phys. Rev. B **68**, 235205 (2003).
[43] H. R. Schober, Phys. Rev. B **39**, 13013 (1989).
[44] F. J. Morin and J. P. Maita, Phys. Rev. **96**, 28 (1954).
[45] D. A. Antoniadis, A. G. Gonzales, and R. W. Dutton, J. Electrochem. Soc. **125**, 813 (1978).
[46] W. A. Orr Arienzo, R. Glang, R. F. Lever, R. K. Lewis, and F. F. Morehead, J. Appl. Phys. **63**, 116 (1988).
[47] J. Murota, E. Arai, K. Kobasyashi, and K. Kudo, Jpn. J. Appl. Phys. **17**, 457 (1978).
[48] J. Murota, E. Arai, K. Kobasyashi, and K. Kudo, J. Appl. Phys. **50**, 804 (1979).
[49] M. Yoshida, E. Arai, H. Nakamura, and Y. Terunuma, J. Appl. Phys. **45**, 1498 (1974).
[50] M. Yoshida, Jpn. J. Appl. Phys. **18**, 479 (1979).
[51] G. D. Watkins, in *Deep Centers in Semiconductors*, edited by S. T. Pantelides (Gordon and Breach, New York, 1986), Chap. 3.
[52] G. D. Watkins, MRS Symposia Proceedings No. 469 (Materials Research Society, Pittsburgh, PA, 1997), p. 139.
[53] A. Ural, P. B. Griffin, and J. D. Plummer, Appl. Phys. Lett. **79**, 4328 (2001).
[54] Y. Nakabayashi, H. I. Osman, T. Segawa, K. Saito, S. Matsumoto, J. Murota, K. Wada, and T. Abe, Jpn. J. Appl. Phys., Part 2 40, L181 (2001).
[55] Y. Nakabayashi, H. I. Osman, K. Yokota, K. Toyonaga, S. Matsumoto, J. Murota, K. Wada, and T. Abe, Mater. Sci. Semicond. Process. **6**, 15 (2003).
[56] S. Matsumoto, S. R. Aid, S. Seto, K. Toyonaga, Y. Nakabayashi, M. Sakuraba, Y. Shimamune, Y. Hashiba, J. Murota, K. Wada, and T. Abe, ECS Transactions **2**, 287 (2006).
[57] R. Car, P. J. Kelly, A. Oshiyama, and S. T. Pantelides, Phys. Rev. Lett. **52**, 1814 (1984).
[58] X.-Y. Liu, W. Windl, K. M. Beardmore, and M. P. Masquelier, Appl. Phys. Lett. **82**, 1839 (2003).
[59] Jianjun Xie and S. P. Chen, J. Phys.: Condens. Matter **11**, 7219 (1999).
[60] Jianjun Xie and S. P. Chen, Phys. Rev. Lett. **83**, 1795 (1999).
[61] M. J. Puska, S. Pöykkö, M. Pesola, and R. M. Nieminen, Phys. Rev. B **58**, 1318 (1998).
[62] M. I. J. Probert and M. C. Payne, Phys. Rev. B **67**, 075204 (2003).
[63] V. Ranki and K. Saarinen, Phys. Rev. Lett. **93**, 255502 (2004).
[64] F. El-Mellouhi, N. Mousseau, and P. Ordejon, Phys. Rev. B **70**, 205202 (2004).
[65] A. Nylandsted Larsen and P. Kringhoj, Appl. Phys. Lett. **68**, 2684 (1996).
[66] S. T. Dunham and C. D. Wu, J. Appl. Phys. **78**, 2362 (1995).

[67] A. Seeger and K. P. Chik, Phys. Status Solidi **29**, 455 (1968).
[68] G. D. Watkins and J. W. Corbett, Phys. Rev. **138**, A543 (1965).
[69] P. Pellegrino, P. Leveque, J. Lalita, A. Hallen, C. Jagadish, and B. G. Svensson, Phys. Rev. B **64**, 195211 (2001).
[70] M. Mikelsen, E. V. Monakhov, G. Alfieri, B. S. Avset, and B. G. Svensson, Phys. Rev. B **72**, 195207 (2005).
[71] G. S. Hwang and William A. Goddard III, Phys. Rev. B **65**, 233205 (2002).